



1 **Developing a tile drainage module for Cold Regions**

2 **Hydrological Model: Lessons from a farm in Southern**

3 **Ontario, Canada**

4

5 **Mazda Kompanizare<sup>\*&#</sup>, Diogo Costa<sup>\*+</sup>, Merrin L. Macrae<sup>&</sup>, John W. Pomeroy<sup>\*</sup>, Richard M. Petrone<sup>&</sup>**

6 **<sup>\*</sup>Centre for Hydrology, University of Saskatchewan, Canmore and Saskatoon, Canada**

7 **<sup>+</sup>Environment and Climate Change Canada, Saskatoon, Canada**

8 **<sup>&</sup>University of Waterloo, Waterloo, Canada**

9 **<sup>#</sup>Corresponding author: kompanizare.mazda@usask.ca**

10

11 **Abstract**

12 Systematic tile drainage is used extensively in agricultural lands to remove excess water and  
13 improve crop growth; however, tiles can also transfer nutrients from farmlands to downstream  
14 surface water bodies, leading to water quality problems. There is a need to simulate the  
15 hydrological behavior of tile drains to understand the impacts of climate or land management  
16 change on agricultural runoff. The Cold Regions Hydrological Model (CRHM) is a physically  
17 based, modular modeling system that enables creating comprehensive models appropriate for  
18 cold regions by including a full suite of winter, spring, and summer season processes and  
19 coupling these together via mass and energy balances. A new tile drainage module was  
20 developed for CRHM to account for this process in tile-drained landscapes that are increasingly  
21 common in cultivated basins of the Great Lakes and northern Prairies regions of North America.



22 A robust multi-variable, multi-criteria model performance evaluation strategy was deployed to  
23 examine the ability of the module with CRHM to capture tile discharge under both winter and  
24 summer conditions. Results showed that soil moisture is largely regulated by tile flow and lateral  
25 flow from adjacent fields. The explicit representation of capillary rise for moisture interactions  
26 between the rooting zone and groundwater greatly improved model simulations, demonstrating  
27 its significance in the hydrology of tile drains in loam soils. Water level patterns revealed a  
28 bimodal behaviour that depended on the positioning of the capillary fringe relative to the tile. A  
29 novel aspect of this module is the use of field capacity and its corresponding pressure head to  
30 provide an estimate of drainable water and thickness of the capillary fringe, rather than a detailed  
31 soil retention curve that may not always be available. Understanding the bimodal nature of soil  
32 water levels provides better insight into the significance of dynamic water exchange between soil  
33 layers below drains to improve tile drainage representation in models.

34

35 Keywords: tile drainage, cold regions, hydrological model, capillary fringe, drainable water,  
36 water level fluctuations

37

38

## 39 **1. Introduction**

40

41 Harmful algal blooms and eutrophication in large freshwater lakes surrounded by agricultural  
42 lands are major environmental challenges in Canada and globally. The transport of nutrients,  
43 particularly phosphorus, in runoff from agricultural fields into rivers, ponds and eventually lakes  
44 is an important contributor to the increased frequency of algal blooms being experienced in



45 North America and elsewhere (Sharpley et al., 1995; Correll, 1998; Filippelli, 2002; Ruttenger,  
46 2005; Schindler, 2006; Quinton et al., 2010). Nutrient transport from agricultural fields can occur  
47 via both surface runoff and tile drainage (Radcliffe et al., 2015), and recent increases in the  
48 frequency and magnitude of algal blooms in Lake Erie in North America have been attributed to  
49 tile drainage (King et al., 2015; Jarvie et al., 2017). Tile drain systems reduce the retention time  
50 of soil water, lessening waterlogging in fields and improving both crop growth and field  
51 trafficability for farmers (Cordeiro and Ranjan, 2012; Kokulan et al., 2019a). However, they are  
52 also important pathways for dissolved and particulate nutrients (Kladvko et al., 1999; Tomer et  
53 al., 2015). It has been estimated that 14% of farmlands in Canada (ICID, 2018) and 45% of fields  
54 in Southern Ontario, Canada (ICID, 2018; Kokulan, 2019) are drained by tile systems. In  
55 Alberta, tile drains have also been used to address salinity issues (Broughton and Jutras, 2013).  
56 Given their importance in hydrological budgets and biogeochemical transport, there is a need to  
57 understand the controlling mechanisms of water and nutrient export from tile systems as an  
58 integral part of the broader, modified hydrological system. The ability to integrate a dynamic  
59 quantification of tile drainage from fields in hydrological models can help understand the relative  
60 importance of this human-induced process as it interplays with an array of other phenomena,  
61 including energy and physical mass balance hydrological processes, climate change, and the  
62 impacts of modified land management practices on runoff and nutrient export.

63         There are several models that can represent tile drainage at the small basin scale, such as  
64 HYPE (Lindstrom et al., 2010; Arheimer et al., 2015), DRAINMOD (Skaggs, 1978, 1980a;  
65 Skaggs et al., 2012), MIKE SHE (Refsgaard and Storm, 1995) and SWAT (Arnold et al., 1998;  
66 Koch et al., 2013; Du et al., 2005; Du et al., 2006; Green et al., 2006; Kiesel et al., 2010). These  
67 models include conceptual components for many key hydrological processes, but research shows



68 that they have been primarily designed and tested for temperate regions (Costa et al., 2020a). In  
69 Canada and other cold regions, some unique hydrological processes such as frozen soil,  
70 snowmelt, rain on snow, and runoff over and infiltration into frozen or partially-frozen soils may  
71 be very important (Rahman et al., 2014; Cordeiro et al., 2017; Pomeroy et al., 1998, 2007; Fang  
72 et al., 2010, 2013). Many hydrological processes, such as the sublimation of snow, energy  
73 balance snowmelt, and infiltration into frozen soils, are strongly affected by temperature and the  
74 phase changes of water, which make many existing models developed for warm regions less  
75 appropriate for regions with cold seasons (Pomeroy et al., 2007; Pomeroy et al., 2013; Pomeroy  
76 et al., 2016; Fang et al., 2010, 2013). Even for temperate regions, the representation of cold  
77 season processes is often underrepresented in models (Costa et al., 2020a).

78         Since the use of tile drainage is becoming popular in many cold regions, it has become  
79 important to integrate such human-induced process in specialized hydrological modelling tools  
80 for these regions, such as the Cold Regions Hydrological Modelling platform (CRHM, Pomeroy  
81 et al., 2007; 2013; 2022). CRHM was initially developed in 1998 to assemble and explore the  
82 hydrological understanding developed from a series of research basins spanning Canada and  
83 elsewhere into a flexible, modular, object-oriented, multiphysics platform for simulating  
84 hydrological processes and basin response in cold regions (Pomeroy et al., 2007; 2022). The  
85 modular CRHM platform allows for multiple representations of forcing data interpolation and  
86 extrapolation, hydrological model spatial and physical process structure and parameter values.  
87 Many existing models typically operate at default daily or monthly time intervals, which is  
88 inadequate for the prediction of many short-duration “flashy” hydraulic responses often observed  
89 in tiles (Puer et al., 2020; Vivekananthan, 2019; Vivekananthan et al., 2019; Lam et al., 2016a,  
90 2016b; Macrae et al., 2019). Indeed, the ability to simulate shorter time intervals (e.g., hourly)



91 facilitates the ability to capture both the rising and falling limbs of tile flow hydrographs, as well  
92 as the magnitude of peak flows, both of which are important to tile drain chemistry and export  
93 (Rozemeijer et al., 2016; Williams et al., 2015, 2016; Macrae et al., 2019).

94 Hydrological process models such as DRAINMOD, MIKE SHE and SWAT use a  
95 combination of empirical and physically based formulations for the simulation of tile flow  
96 derived by Hooghoudt (1940), Kirkham (1957), van Schilfgaarde (1974), Bouwer and van  
97 Schilfgaarde (1963) and Skaggs et al., (1978). Such formulations contemplate both cases where  
98 the soil water level is below and above the ground surface (Kirkham, 1957). In contrast,  
99 simulations of tile drainage in other models such as HYPE use empirically-derived recession  
100 curves (Eckersten et al., 1994) to simulate tile flow and water levels. In cases where there is a  
101 need for more focus on soil matrix hydrology and less need for understanding the relative  
102 contribution of tiles (and its interplay) with other catchment-scale mass balance hydrological  
103 processes, modellers tend to use specialised porous-media PDE-based (partial differential  
104 equation-based) numerical models such as HYDRUS (Simunek et al., 2011) and MACRO  
105 (Larsbo and Jarvis, 2003).

106 The amount of water transported by tiles depends on soil moisture dynamics and the  
107 positioning of the water table, which are in turn affected by many factors, including soil type,  
108 surface topography and morphology, as well as the local climate and the hydrologic  
109 characteristics of the field (Frey et al. 2016; Klaiber et al., 2020; Coelho et al., 2012; King et al.,  
110 2015). Thus, to provide reliable estimations of water from farmland via surface runoff and tile  
111 flow, models must be able to predict soil moisture and the soil water level accurately (Brockley,  
112 1976; Rozemeijer et al., 2016; Javani-Jouni et al., 2018). Many studies have shown that in some  
113 soil types, including silty loam and clay loam soils, the drainable water is less than expected



114 based on the effective porosity (*e.g.*, Skeggs et al., 1978; Raats and Gardner, 1974). Raats and  
115 Gardner (1974) have argued that the calculation of drainable porosity requires knowledge of the  
116 soil water level position and the distribution of soil moisture above the water level. Skeggs et al.  
117 (1978) added that the calculation of drainable porosity should take into account “the unsaturated  
118 zone drained to equilibrium with the water table”. However, because the soil column is often  
119 composed of different soil layers with varying physical characteristics, drainable porosity varies  
120 with evapotranspiration rate, soil water dynamics and the water level depth (Logsdon et al.,  
121 2010; Moriasi et al., 2013). In a sandy loam soil, Lam et al. (2016a, 2016b) demonstrated that  
122 tile drainage was not initiated until soils were at or above field capacity. Williams et al. (2019)  
123 observed in the American Midwest that tile drainage was not initiated until the field storage  
124 capacity had been exceeded. It has also been shown that despite the presence of tile drains, the  
125 soil above the tile may not drain appreciably into the tile following an event and may remain at  
126 or above field capacity (Skaggs et al., 1978; Lam et al., 2016a). Therefore, the soil drainable  
127 water content may be considerably smaller than the storage capacity. This is related to matric  
128 potential within the vadose zone, which is driven by the soil characteristics but can also be due to  
129 the development of a capillary fringe that reduces the rate of vertical percolation through the  
130 unsaturated zone, reducing tile flow (Youngs, 2012). Despite this evidence, some saturated flow  
131 models that simulate tile flow overlook the effect of capillary rise and over-estimate the soil  
132 drainable water. Other models that represent unsaturated flow (*i.e.* HYDRUS 3D, Simunek et al.,  
133 2011) using Richard’s Equation (Richards, 1931) capture the effect of capillary rise and  
134 saturation-pressure variation within the soil profile and assess the soil drainable water more  
135 accurately. Although the effect of capillary rise is considered in DRAINMOD through the  
136 concept of drainable porosity (that is represented as a “water yield”) (Skaggs, 1980b), and is



137 calculated for layered soil profiles (Badr,1978), it requires detailed information surrounding the  
138 soil water characteristic curve (Skaggs, 1980b). It is indeed optimal to use soil-specific water  
139 characteristic curves; however, Twarakawi et al. (2009) found that it was possible to employ  
140 average representative values from the soil water characteristic curve to represent soil drainable  
141 water where a soil-specific curve is not available.

142 In this study, a new tile drainage module was developed and incorporated within the  
143 physically based, modular Cold Regions Hydrological Modelling (CRHM) platform (Pomeroy et  
144 al., 2022) to enable hydrological simulations in tile-drained farm fields in cold agricultural  
145 regions. In this module, considerations were explicitly included for the effect of capillary rise  
146 and annual groundwater water table fluctuations on drainable soil water storage. The use of field  
147 capacity and pressure head (Twarakawi et al., 2009) to modulate soil drainable water across the  
148 soil profile, including the capillary fringe region, is an innovative aspect of the model that has  
149 been demonstrated to negate the need for water characteristic curves.

150

## 151 **2. Materials and Methods**

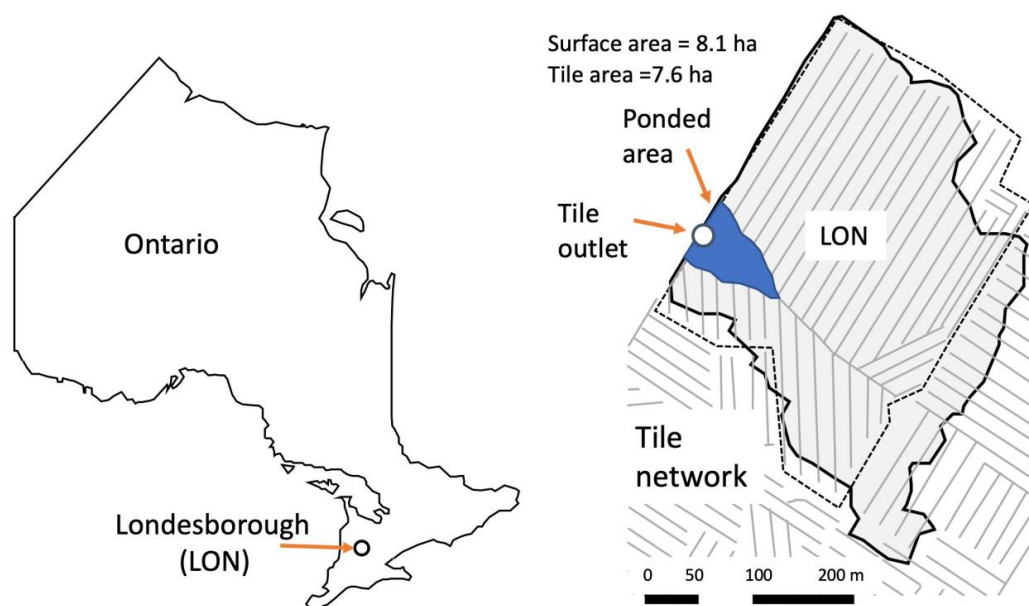
### 152 *2.1 Study area*

153 The study site is a ~10 ha farm field located near Londesborough, LON (UTM 17T 466689m E,  
154 4832203m N), Ontario (Fig. 1a). Mean annual precipitation recorded in this region is 1247 mm  
155 (ECCC, 2020). Mean air temperature is 7.2 °C, with annual maxima in July (25.9 °C) and  
156 minima in January (-10.2 °C), (ECCC, 2020). Soil texture has been identified as Perth clay loam  
157 (Gr. Br. Luvisolic), with a slope between 0.2 and 3.5%. The field is systematically drained with a  
158 tile depth of 0.9 m and a spacing of 14 m (laterals). The tile network collects infiltrated water  
159 from about 75% of the field (~ 7.6 ha), which is discharged via a common tile outlet (main). The



160 field is a corn-soy-winter wheat rotation with cover crops and rotational conservation till  
161 (shallow vertical tillage every three years). Additional details related to farming practices are  
162 provided in Plach et al. (2019) and soil characteristics are provided in Plach et al. (2018a) and  
163 Plach et al. (2018b). The outlets of the surface and tile flows are located at the edge of the field  
164 and drain into an adjacent field (Fig. 1b). Water tends to accumulate in a topographic low in the  
165 field, in front of the field outlet during snowmelt or high-intensity rainfall events (see ponded  
166 area, Fig. 1b). This zone coincides with the tile drain main pipe and is not a zone of groundwater  
167 discharge.

168



169

170 a)

b)

171 b) Figure 1. (a) Location of the study area in South of Ontario and the (b) Londesborough (LON) farm with its tile network.

172

173





174 2.2 *CRHM: The modelling platform*

175 The modular CRHM platform includes options for empirical and physically based calculations of  
176 precipitation phase, snow redistribution by wind, snow interception, sublimation, sub-canopy  
177 radiation, snowmelt, infiltration into frozen and unfrozen soils, hillslope water movement, actual  
178 evapotranspiration, wetland fill and spill, soil water movement, groundwater flow and  
179 streamflow (Pomeroy et al., 2007; 2022). Where appropriate, it calculates runoff from rainfall  
180 and snowmelt as generated by infiltration excess and/or saturated overland flow, flow over  
181 partially frozen soils, detention flow, shallow subsurface flow, preferential flow through  
182 macropores and groundwater flow. Water quality can also be simulated (Costa et al., 2021).  
183 Modules of a CRHM model can be specific to basin setup, such as delineating and discretizing  
184 the basin, conditioning observations for extrapolation and interpolation in the basin, or are  
185 process-support algorithms such as for estimating longwave radiation, complex terrain wind  
186 flow, or albedo dynamics, but most commonly address hydrological processes such as  
187 evapotranspiration, infiltration, snowmelt, and streamflow discharge. CRHM discretizes basins  
188 into hydrological response units (HRU) for mass and energy balance calculations, each with  
189 unique process representations, parameters and position along flow pathways in the basin. HRU  
190 are connected by blowing snow, surface, subsurface and groundwater flow and together generate  
191 streamflow which is routed to the basin outlet. CRHM does not require a stream within a  
192 modelled basin. The feature allows CRHM to model the hydrology of regions dominated by  
193 storage and episodic runoff, such as agricultural fields.

194 Although CRHM has capabilities to represent many different processes, not all processes  
195 must be represented in all situations. The modular design of the CRHM platform enables the user  
196 to activate or inactive specific processes to optimize the model for a particular situation. For  
197 example, in the current study, blowing snow was not employed as it does not appear to be



198 significant at the study site (periodic snow surveys showed relatively uniform snow cover).  
199 Preferential flow into tile drains was not developed for the current simulation as although it is a  
200 key process in heavy clay soil, as it does not appear to be a significant driver of preferential flow  
201 into tile drains in coarse textured soil (Pluer et al., 2020; Macrae et al., 2019). Freeze-thaw  
202 processes in soil were also not employed here as there is very little seasonal soil frost in the  
203 temperate Great Lakes region due to the persistent snow cover, and where soil frost occurs, it is  
204 restricted to brief periods and shallow depths (above 10 cm depth) (Macrae unpublished data).

205

### 206 2.3 *Observations and input data for the model*

207 Tile flow, soil water level (water table position) and surface flow were measured at the site  
208 between Oct. 2011 and Sept. 2018 at 15-minute intervals. It was not possible to install more than  
209 one measuring station at the site due to farming activity, so water table position and soil moisture  
210 were measured at the field edge, approximately at the midpoint of the field. Tile flow rates were  
211 determined using simultaneous measurements of flow velocity and water level in the tile main  
212 pipe at the edge of the field (Table A1, Appendix A), with an additional barometrically-corrected  
213 pressure transducer (Table A1) for periods when the flow sensor did not function. Surface runoff  
214 naturally exits the field at one location. However, to facilitate its measurement, the edges of the  
215 field were equipped with berms (1/2 plywood sheets, installed vertically above and below the  
216 ground), directing surface runoff through a culvert (45 cm diameter). Surface runoff through the  
217 culvert was also measured using a Hach Flo-tote sensor and FL900 logger. The soil water level  
218 in the field was measured at the edge of the field, located midway between the topographic high  
219 and low points of the field, using a baro-corrected pressure transducer.



220 Air temperature, wind speed, air relative humidity, incoming solar irradiance and rainfall were  
221 also measured at the site at 15-minute intervals and used to force the model. Variable names and  
222 their symbols in CRHM are listed in Appendix B. The air temperature, wind speed and incoming  
223 solar radiance measurements were collected 1 m above ground using a Temperature Smart  
224 Sensor S-THB-M002, Wind Smart Sensor Set S-WSET-M002 and a Solar Radiation Sensor  
225 (Table A1). Rainfall and relative humidity were measured via a tipping bucket rain gauge (Table  
226 A1) and a RH Smart Sensor (Table A1). These observations were continuously recorded  
227 throughout the study period, with the exception of brief periods of instrument failure and  
228 maintenance, when data from nearby stations (Table T1, Supplementary Material) was  
229 substituted using the double mass analysis method (Searcy and Hardison, 1960).  
230 Although rainfall was recorded continuously at the field site, snowfall data was not. Snowfall  
231 data was obtained from nearby stations (Wroxeter-Davis and Wroxeter, Environment Canada,  
232 2021), located 31.7 km from the field site. Periodic snow surveys done at the site found that data  
233 from the nearby stations was a close approximation of snow at the field site. Hourly precipitation  
234 data from Wroxeter-Geonor were used for the period between 2015 and 2018, whereas daily data  
235 from the Wroxeter station and the daily pattern of snowfall from Wroxeter-Geonor were  
236 combined for the period between 2011 and 2014 for reconstruction of the missing hourly  
237 snowfall time series based on the method presented by Waichler and Wigmosta (2003).

238

#### 239 *2.4 Development of the new tile module*

240 A Tile Drainage Module (TDM) was developed within CRHM with the goal of adding the ability  
241 to simulate tile flow and the resulting soil water levels at an hourly time scale. CRHM was  
242 forced with hourly precipitation, air temperature, solar radiation, wind speed and relative



243 humidity to calculate hydrological states and fluxes in HRUs and the basin. The model requires  
244 parameterizations that specify the hydraulic and hydrological properties of the soil, including its  
245 thickness, saturated hydraulic conductivity (K), and surface cover. CRHM calculates water  
246 storage and fluxes between HRUs, as well as vertical fluxes amongst different hydrological  
247 compartments (within each HRU) that include snow, depressional storage, different soil layers,  
248 and groundwater.

249 Based on the simulation of soil moisture performed by the original CRHM “Soil” module, TDM  
250 calculates the dynamic tile flow rate that, in turn, feeds back to soil moisture at each time step.  
251 The presence of a capillary fringe (sometimes referred to as the tension-saturated zone within the  
252 soil profile) and its effects are considered by limiting the amount of drainable soil water. TDM  
253 uses specific site-specific information about the tile network, such as the tile depth, diameter and  
254 spacing, together with a parameterisation that translates the hydrological effect of the soil  
255 capillary fringe (CF), if present, into two state variables, CF thickness and CF drainable water.  
256 These two state variables are used to limit the fraction of the soil moisture that can freely drain to  
257 the tiles.

258

#### 259 *2.4.1 Soil moisture and water level*

260 The TDM uses the water quality soil module or soil module (*WQ\_soil* or *Soil*), which divides the  
261 soil column into two layers: a recharge layer where evapotranspiration and root uptake generally  
262 take place and a deeper layer that connects to the groundwater system. Since CRHM's state  
263 variable for soil moisture is soil water storage volume (Fig. 2a), the model results were converted  
264 into water level elevation above the semipermeable layer (Table B1, Appendix B; see Fig. 2b for  
265 comparison with soil water level observations) by dividing volumetric soil moisture content



266 (Table B1) by soil porosity (Table B1) for the cases with no capillary fringe above the soil water  
267 level. Additional steps were taken for periods when a capillary fringe developed (discussed  
268 below).

269

#### 270 2.4.2 Capillary fringe and drainable water

271 Soil moisture in the capillary fringe is equal to the field capacity ( $\theta_{fc}$ ) (Bleam, 2017, Sect. 2.4).

272 Therefore, while the positioning of the capillary fringe responds dynamically to the matric

273 potential, the saturation profile within the capillary fringe remains constant, as well as its

274 thickness because it only depends on the pressure head (capillary forces) that are related to the

275 grain size distribution and field capacity ( $h_{fc}$ ) as introduced by Twarakawi et al. (2009).

276 Therefore, the drainable water in the capillary fringe becomes the difference between saturation

277 ( $\theta_s$ ), computed dynamically in CRHM, and  $\theta_{fc}$ , which corresponds to the water held by capillary

278 forces at field capacity (Fig. 2). Accordingly, Fig. 2 shows the schematic soil characteristic curve

279 for the three water level conditions contemplated in the model.

280 1. *Condition 1* is when the matric head is at the surface and the soil is completely saturated;

281 2. *Condition 2* is when the matric head drops but the upper boundary of the capillary fringe  
282 is at the soil surface; and

283 3. *Condition 3* is when water level drops further and the upper boundary of the capillary  
284 fringe drops beneath the surface.

285 In essence, the soil is completely saturated ( $\theta_s$ ) in *Condition 1*. Between *Conditions 1* and 2, the

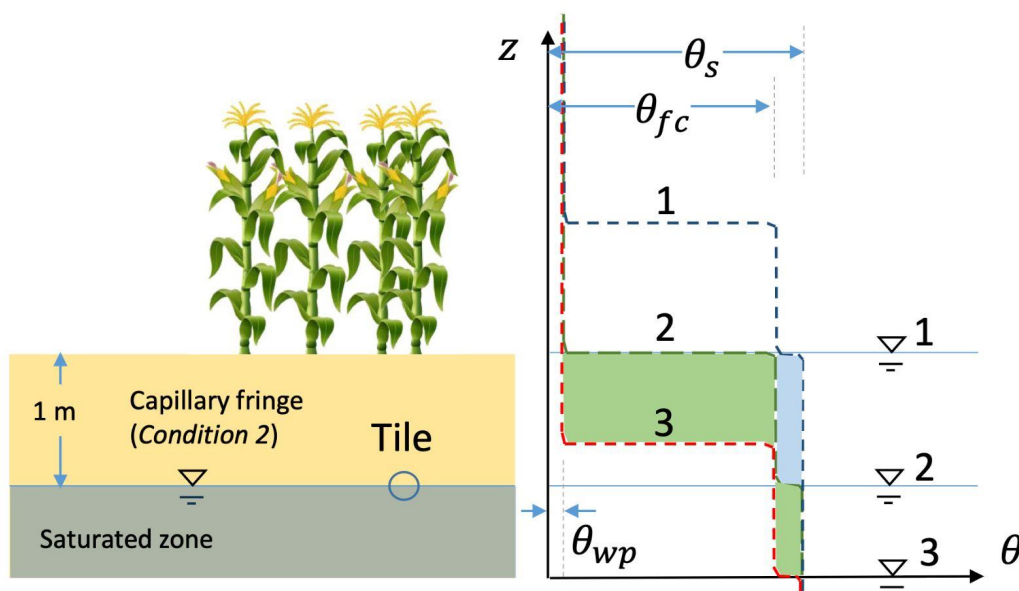
286 capillary fringe occupies the entire soil column above the water level; thus, it can only release

287 the volume of water corresponding to  $\theta_s - \theta_{fc}$  or  $\varphi_c$  (dimensionless). Between *Conditions 2* and 3,

288 two layers with distinct hydraulic characteristics develop: (1) the top one at  $\theta_{wp}$  that releases



289 water up to  $\theta_{fc}-\theta_{wp}$ , and (2) the lower one that corresponds to the capillary fringe and can  
 290 release up to the volume of water corresponding to  $\theta_s-\theta_{fc}$  or  $\varphi_c$ .



291  
 292 Figure 2. Schematic representation of the capillary fringe above the soil water level assuming a 1-m thickness (for demonstration  
 293 purposes). The soil characteristic curves are shown for the three water level conditions considered: water level at the (1) surface,  
 294 (2) intermediate depth, and (3) deeper depth. Two transitional drops can be seen in the characteristic curves, one from saturation  
 295 ( $\theta_s$ ) to field capacity ( $\theta_{fc}$ ) (between *Conditions 1* and 2) and one from field capacity to wilting point ( $\theta_{wp}$ ) (between *Conditions*  
 296 2 and 3). The colored areas (green and blue) of the right panel correspond to the amount of water that can be released between  
 297 *Conditions 1* and 2 (blue) and between *Conditions 2* and 3 (green).

298

299

### 300 2.4.3 Tile flow calculation

301 A modified version of the Hooghoudt equation was used to calculate tile flow (Smedema et al.,  
 302 2004), which presumes no surface ponding, an assumption that generally holds at the study site  
 303 (Eq. 1), where water ponds only during very wet periods and on a small portion of the study site



304 (see Fig. 1b). Hooghoudt's equation (Hooghoudt, 1940) is a steady state, physically based  
305 equation for saturated flow toward the tile drain. Flow estimates are provided based on the  
306 hydraulic conductivity of the soil and matric potential. It allows different saturated hydraulic  
307 conductivities for the layers above (AL) and below (BL) the tile (Fig. S1). In the particular case  
308 of the case study site, soil surveys have reported almost the same soil type (Loam) down to the  
309 depth of 90 cm (e.g. Van Esbroeck et al., 2016; Plach et al., 2018b), which was parameterized in  
310 the model set up as,

311

$$312 \quad q = \frac{8 \times K_2 \times d \times h}{L^2} + \frac{4 \times K_1 \times h^2}{L^2}, \quad (1)$$

313

314 where  $K_1$  and  $K_2$  are respectively the saturated hydraulic conductivity in the upper and lower  
315 layers in  $\text{mm h}^{-1}$ ;  $L$  is the tile spacing in mm;  $h$  is the soil water level elevation above the tile in  
316 mm,  $d$  is the lower layer thickness in mm (Fig. S1), and  $q$  is the predicted tile flow in  $\text{mm h}^{-1}$ .  
317 The only variable that is dynamically updated by CRHM is  $h$ . Equation (1) is used to estimate  
318 the tile flow.

319

#### 320 2.4.4 Calculation of the effect of tile flow on soil moisture and water levels

321 The simulated tile flows (see Sect. 2.3.3) are subtracted from the soil moisture. To calculate a  
322 water level from soil moisture, a threshold soil moisture content ( $sm_t$ ) is defined, which consists  
323 of drainable water in the soil when the upper boundary of the capillary fringe is at the surface  
324 (Condition 2, Fig. 2) and can be calculated as:

325

$$326 \quad sm_t = sm_{max} - (C_t \times \varphi_c), \quad (2)$$



327

328 where  $sm_{max}$  is the maximum soil moisture and  $C_t$  is the capillary fringe thickness in mm.

329 However, since the hydrological conditions of the soil are markedly different between the two

330 transitional situations described in Sect. 2.3.2 and Fig. 2 (*Condition 1* to 2 and *Condition 2* to 3),

331 a step function had to be considered for determination of the matric potential:

332

$$333 \quad SWL = \begin{cases} \frac{sm_t - (C_t \times ((\varphi_s - \varphi_c) + \theta_{wp}))}{\varphi_s + \theta_{wp}} + \frac{sm - sm_t}{\varphi_c} & , \text{if between Conditions 1 and 2} \\ \frac{sm_{max}}{\varphi_s + \theta_{wp}} - \left( \left( \frac{sm_t - sm}{\varphi_s} \right) + C_t \right) & , \text{if between Conditions 2 and 3} \end{cases} \quad (3)$$

334

335 where  $SWL$  is soil water level elevation in mm from the bottom of the soil, and  $sm$  is soil

336 moisture in the given time step in mm. Equation (3) is determined based on soil moisture curves

337 in Fig. 2 and water level *Conditions 1-3* discussed in Sect. 2.3.2. In Fig. 2, the first and second

338 parts of Eq. (3), which refer to *Conditions 1* to 2 and 2 to 3, respectively, correspond to the

339 volumes of soil water highlighted in “blue” and “green.”

340

#### 341 2.4.5 Lower semi-permeable soil layer and periodicity in annual groundwater levels

342 This model application focused on the study site field without including other adjacent areas.

343 This was possible because years of field monitoring at this site have demonstrated that there is no

344 observable surface flow into the site from adjacent farms. The tile network is restricted to the

345 field and is not connected to tile drains or surface inlets in adjacent fields. However, field soil

346 water level observations show evidence of annual groundwater level periodicity/fluctuation (Rust

347 et al., 2019) that are sinusoidal in nature and cannot be neglected. Some studies predict the





348 annual groundwater oscillations or the annual responses of groundwater to precipitation by using  
349 sine and cosine functions (De Ridder et al., 1974; Malzone et al., 2016; Qi et al., 2018). De  
350 Ridder et al. (1974) studied the design of the drainage systems and described the seasonal  
351 groundwater fluctuations observed in wells using sinusoidal curves. Malzone et al. (2016) used a  
352 sine function to predict annual groundwater fluctuations in the hyporheic zone. Qi et al. (2018)  
353 and Rust et al (2019) used a cross-wavelet transform, consisting of the superposition of sine and  
354 cosine curves, to predict shallow groundwater response to precipitation at the basin scale. This  
355 approach was used in this application to simulate annual fluctuations in groundwater water  
356 tables, in Eq. (4), with a period of 1 year, minimums around the middle of the growing season  
357 (mid-July), and maximums in the cold season (early February). This translates into the lowering  
358 of the matric potential during the growing season, causing soil water seepage, and an elevated  
359 matric potential during the non-growing season, causing an increase in the soil moisture  
360 consistent with field observations.

361

$$362 \quad G_{y,i} = \left[ A \times \sin \left( \frac{(T_s - D_d \times 24) \times 360}{24 \times 365.25} \right) - B \right] \times f_{y,i} \quad (4)$$

363

364 where  $T_s$  is the time step number,  $D_d$  is a time delay in days,  $A$  is the amplitude of the soil water  
365 level fluctuation, and  $B$  is an intercept factor.  $f_{y,i}$  is a seasonal factor. The sine function  
366 coefficient ( $D_d$ ,  $A$ , and  $B$ ) and seasonal factor were adjusted for the whole period and for each  
367 year through model verification and shown in Table 1. Appendix C provides more details on the  
368 implementation of Eq. (4).



369

370 2.5 *Model application and multi-variable, multi-metric validation*

371 The study site is a relatively small field, and 2 HRUs revealed sufficient to capture its  
372 hydrological dynamic in CRHM. The HRUs represent (1) the area immediately upstream of the  
373 outlet where surface ponding occurs (depression storage); and (2) the remaining field (Fig. 3).  
374 The maximum ponding capacity of HRU 1 was estimated using the spatially distributed  
375 hydrodynamic model FLUXOS-OVERFLOW (Costa et al., 2020b). The CRHM model and new  
376 TDM module were set up using the information described in Table 1. Soil textures at the LON  
377 site measured in a 25m grid across three soil depths (0-25 cm, 25-50 cm, and 50-100 cm)  
378 averaged 29% sand, 48% silt, and 23% clay (Ontario Ministry of Agriculture, Food and Rural  
379 Affairs Soil Team, unpublished data). This soil grain size distribution corresponds with a soil-  
380 saturated hydraulic conductivity of  $\sim 0.56 \text{ cm h}^{-1}$  ( $\sim 10^{-2.5}$ ) (Garcia-Gutierrez et al., 2018), which  
381 was implemented in CRHM ( $0.5 \text{ cm h}^{-1}$ ), corresponding to a field capacity of 0.03 and  $h_{fc}$  of  
382  $\sim 0.8 \text{ m}$  (Twarskawi et al., 2009, based on a drainage flux of  $0.1 \text{ cm d}^{-1}$ ).

383

384 A robust multi-variable, multi-metric model evaluation strategy was deployed to verify the  
385 capacity of the model to predict tile flow and its impact on the local hydrology. The state  
386 variables examined were tile flow, surface flow, and matric potential. The multi-metric approach  
387 contemplated four different methods, namely the Nash-Sutcliffe efficiency (*NSE*), Root-Mean-  
388 Square Error (RMSE), Model Bias (Bias), Percentage Bias (PBias), and RMSE-observation  
389 standard deviation ratio (RSR). See Appendix A for more details about the methodology used. It  
390 is generally assumed that  $NSE > 0.50$ ,  $RSR \leq 0.70$ , and *PBias* in the range of  $\pm 25\%$  are  
391 satisfactory for hydrological applications (Moriiasi et al., 2007). Hourly values were used in these



392 calculations, which departs from the daily and monthly analyses typically reported for these  
 393 types of models. Although this is a challenging proposition, it is an important one as it  
 394 constitutes a necessary step forward toward more detailed, accurate, and advanced models for  
 395 these regions. For example, Costa et al., 2021 noted that the successful extension of hydrological  
 396 models to water quality studies relies on their ability to operate at small time scales in order to  
 397 capture intense, short-duration storms that may have a disproportional impact on the runoff  
 398 transport of some chemical species such as phosphorus – in essence to capture hot spots and hot  
 399 moments for flux generation.

400

401

402 Table 1. Key model parameters in CRHM for representation of the LON site.

403

Model Parameter	Value	Unit	Source	Adjusted/Calibrated	Comment
Soil depth	2	m		No	Assumed
Semipermeable layer depth	3	m		No	Assumed
Tile depth	0.9	m		No	Farmer/Blueprints of the field
Corn root depth	0.5	m		No	Online sources
Soil recharge zone thickness	0.5	m		No	Based on the root depth
Tile spacing	14	m		No	Farmer/Blueprints of the field
Soil porosity (soil drainable water)	0.045			Yes	Adjusted
$\varphi_s$					
K in below layer	5	mm h <sup>-1</sup>		Yes	Adjusted
K in above layer	5	mm h <sup>-1</sup>		Yes	Adjusted
Capillary fringe thickness	0.8	m		Yes	Adjusted

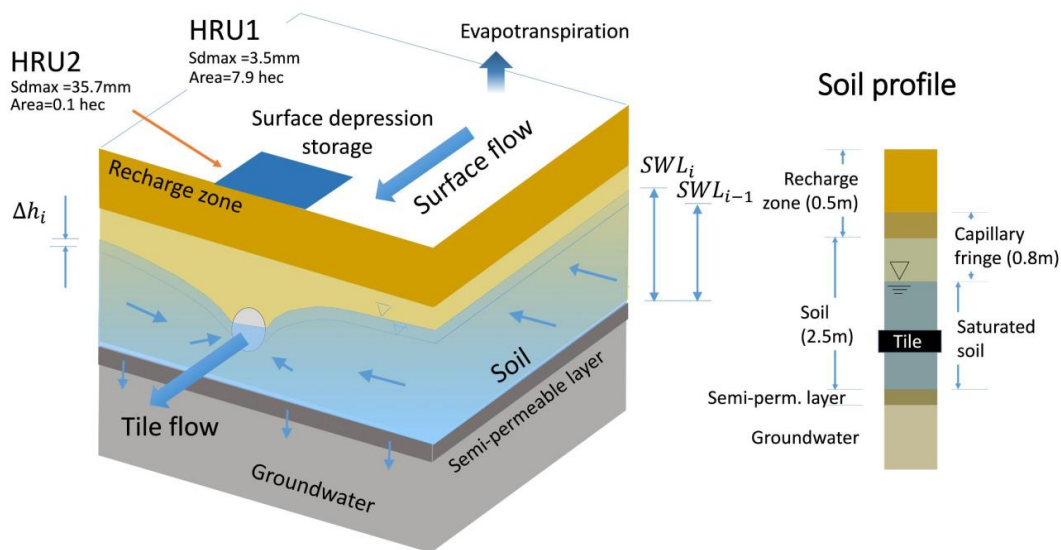


Capillary fringe drainable water $\varphi_c$	0.03		Yes	Adjusted
Surface depression in small area close to farm surface flow outlet (HRU2)	35	mm	Yes	Calculated
Surface depression in rest of the area (HRU1)		mm	No	Calculated
Surface area of HRU1		m <sup>2</sup>	No	Field observations and DEM
Surface area of HRU2		m <sup>2</sup>	No	Field observation and DEM
Soil module name in CRHM	WQ_soil		No	
Infiltration module name in CRHM	GreenAmpt		No	
Soil type in GreenAmpt module	5		Yes	Adjusted
Saturated K in GreenAmpt module	6	mm h <sup>-1</sup>	Yes	Adjusted
Soil wilting point	0.025		Yes	Adjusted
$A$ , in sine function	0.025	mm h <sup>-1</sup>	Yes	Adjusted
$B$ , in sine function	-0.005	mm h <sup>-1</sup>	Yes	Adjusted
$D_d$ , in sine function	15	d	Yes	Adjusted
$f_{2012,2}$ (Seasonal factor, sine function)	2.0		Yes	Adjusted
$f_{2015,2}$ (Seasonal factor, sine function)	1.8		Yes	Adjusted
$f_{2016,2}$ (Seasonal factor, sine function)	2		Yes	Adjusted
$f_{2017,2}$ (Seasonal factor, sine function)	1.4		Yes	Adjusted
$f_{y,i}$	1		No	By default for $y = 2012$ to $2017$ and $i = 1, 2$

404

405

406



407

408 Figure 3 a) Schematic conceptual view of the CRHM model configuration, including soil layers, soil water level, groundwater,  
409 and tile flow.; and b) soil profile, including the capillary fringe and its location relative to the soil and tile.

410

### 411 3. Results

412

#### 413 3.1 Tile flow

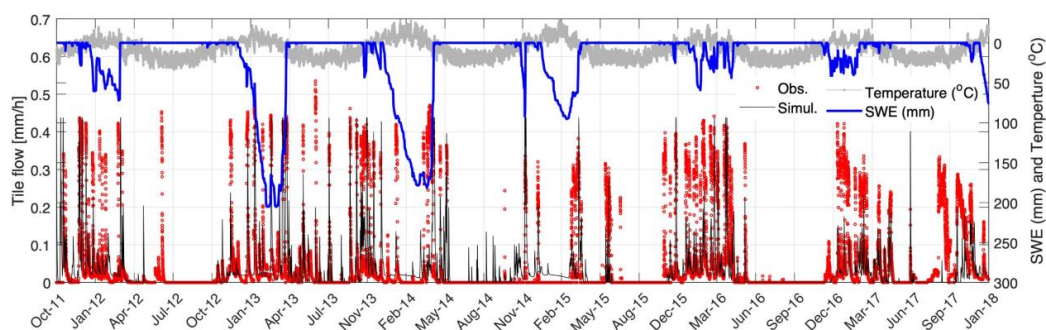
414 The model was able to capture most tile flow events, both in terms of the timing and magnitude  
415 of peak flows and the most important seasonal patterns (Fig. 4). For example, the almost  
416 complete absence of tile flow during the growing season (May to September) was captured. The  
417 simulated flow peaks generally have a good agreement with observations, as well as the low flow  
418 or base flows during cold periods (December-March). The ascending and descending limbs of  
419 the response signal are also adequately predicted.

420

421 Results show that tile flows generally occur during snowmelt events, as indicated by the  
422 synchrony between snow water equivalent (SWE) depletion and tile flow. The maximum



423 snowpacks (or snow water equivalent, SWE) were markedly smaller during the winters of 2016  
424 and 2017 when compared with those of 2013 to 2015. However, this did not necessarily translate  
425 into lower tile flows as precipitation also occurred as rain during these seasons.



426

427 Figure 4 Comparison between observed and simulated tile flows, simulated SWE, and observed air temperature in the LON site.

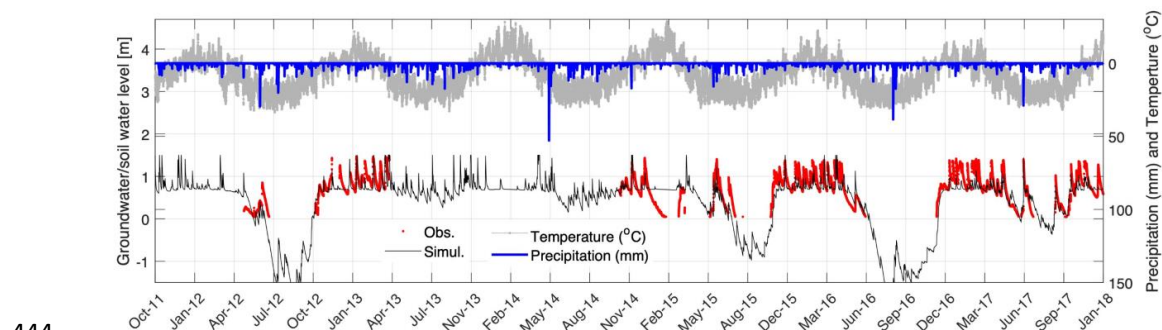
428

### 429 3.2 Soil water levels

430 Simulated and observed soil water levels (m) are compared in Fig. 5, alongside air temperature  
431 and precipitation observations. Despite the observation gaps, the model agrees well with  
432 observations. Above tile drains, water fluctuations are controlled by infiltration/recharge, tile  
433 flow, groundwater flow, and matric potential that affects the drainable water from the capillary  
434 fringe. In contrast, tiles do not withdraw water from the soil layer below the tile pipe. This causes  
435 flashier soil moisture responses above the tile that are captured well by the model. During the  
436 growing season, both the observed and simulated soil water levels drop abruptly because of the  
437 seasonal lowering of the regional groundwater water table. In the growing seasons of 2012, 2015  
438 and 2016, which were dry years, large drops in the soil water level were observed, whereas in  
439 other more wet years such as 2013 and 2014, seasonal water level declines were smaller. The  
440 seasonal declines in water level during the growing season led to a cessation in tile flow in most  
441 years (Fig. 4, 5), even following rainfall events. For example, there was a large precipitation



442 event (~35 mm) in the growing season of 2016 that did not produce tile flow (apparent in both  
443 model and observations).



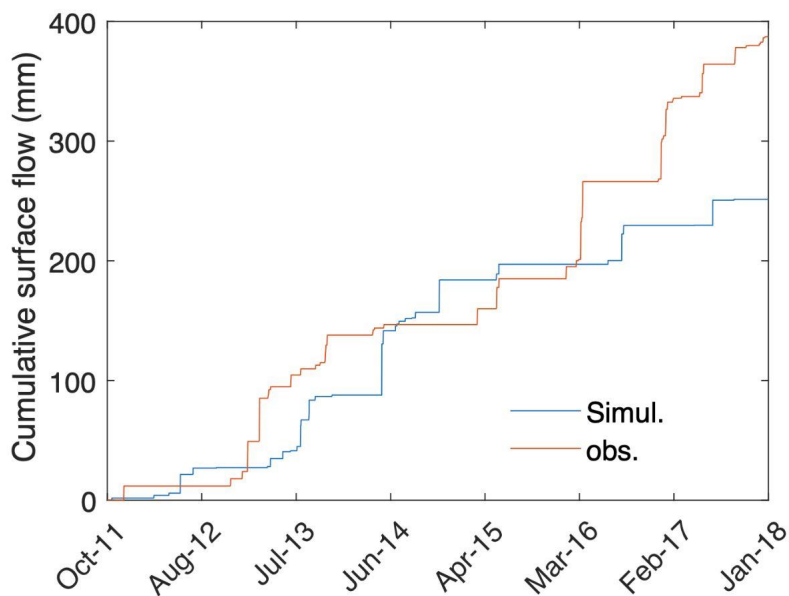
444

445 Figure 5 Time series of the simulated and observed water level in soil along with the observed temperature and precipitation. The  
446 horizontal line shows the depth of the tile pipe.

447

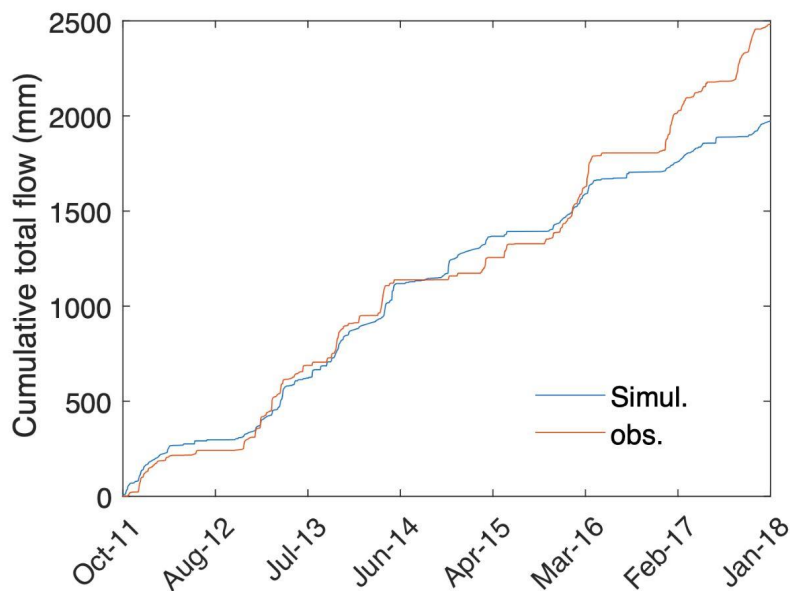
### 448 3.3 Surface flow and total flow

449 The model was not able to capture the observed surface flow as satisfactorily as it captured tile  
450 drainage (Fig. 6a). Some of the possible reasons are uncertainties in the measurements of surface  
451 flow due to ponding in surface depressions on the field, which impeded the drainage of some of  
452 the surface runoff (see Fig. 1). However, the model performance improves considerably when  
453 both runoff and tile flow are combined (referred to as total flow, Fig. 6b). Indeed, most of the  
454 flow from the field was through tile drains (80% in 5-year average) rather than surface runoff  
455 (20% in 5-year average, Plach et al., 2019). The underestimation of both cumulative total and  
456 surface flows during 2017 and 2018 is possibly due to the removal of the blockage in tile pipes in  
457 early 2017 that may have affected both surface and tile flows.



458

459 a)



460

461 b)

462 Figure 6 Observed and simulated cumulative surface flow (a) and total flow (b) with their performance coefficients.





463

464 *3.4 Overall model performance*

465 The model performance was calculated based on hourly data for various model outputs (Table  
 466 2). The results confirm that the model is robust in the sense that it can captures the main patterns  
 467 of tile flow, surface flow, and matric potential levels. The PBias values are below 25% for most  
 468 of the fluxes and cumulative fluxes. The RSR values are also generally below 0.82. The NSE  
 469 values are positive and above 0.3 for most fluxes, except for surface flow, where the model  
 470 exhibited some difficulties.

471

472 Table 2 Performance coefficients for surface flow, tile flow and soil water level as well as total (tile+surface) flow and the  
 473 cumulative surface, tile and tile+surface flows.

<b>Performance coefficients</b>	<b>Surface flow (mm h<sup>-1</sup>)</b>	<b>Tile flow (mm h<sup>-1</sup>)</b>	<b>SWL (m)</b>	<b>Total flow (mm h<sup>-1</sup>)</b>	<b>Cumulative Tile flow (mm)</b>	<b>Cumulative Surface flow (mm)</b>	<b>Cumulative Total Flow (mm)</b>
NSE	-2.29	0.31	0.49	-1.38	0.98	0.85	0.96
RMSE	0.27	0.08	0.26	0.30	111.13	55.61	151.08
Bias	0.54	0.24	0.14	0.28	0.026	0.22	0.047
PBias	21.77	17.91	10.46	18.63	2.05	15.15	3.99
RSR	1.82	0.83	0.71	1.54	0.16	0.39	0.20

474

475



476 3.5 *Presence of capillary fringe: effects and hypotheses*

477 Results show that the thickness and vertical positioning of the capillary fringe have a strong  
478 impact on the amount of drainable soil water that can flow into tiles. To investigate this effect  
479 further, we examined the response of the tile flow and soil moisture to changes in the capillary  
480 fringe. It should be noted that although this thickness may slightly change depending on the soil  
481 type and water retention curves (Skaggs et al., 1978), the model assumed a constant value given  
482 the catchment-scale nature of the simulations and myriad of processes contemplated. However,  
483 despite the simplification, the vertical positioning of the capillary fringe was still computed and  
484 enabled a dynamic (time-dependent) calculation of the drainable soil water that is available for  
485 tile drainage over time.

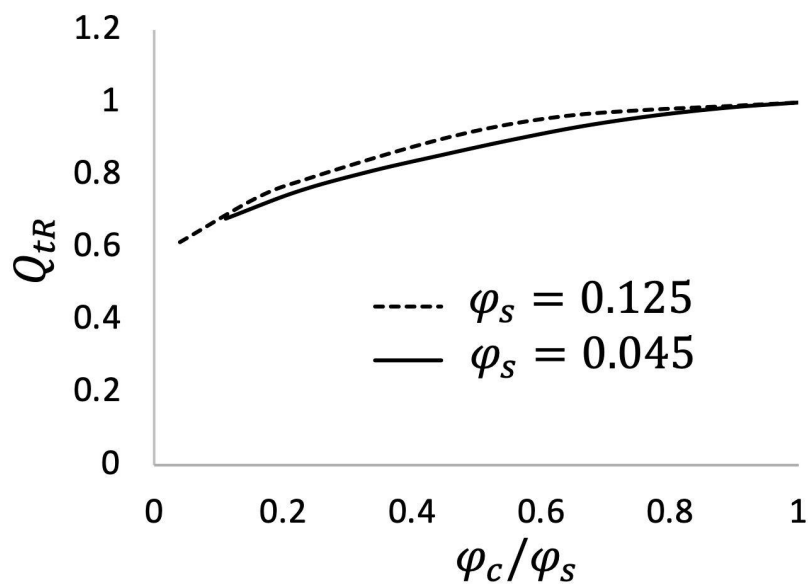
486

487 *Effect of capillary fringe on tile flow*

488 Figure 7a relates the simulated normalized total cumulative tile flow ( $Q_{tR}$ , total tile flow divided  
489 by the total tile flow when there is no influence of capillary fringe) to capillary fringe drainable  
490 water ( $\varphi_{CR} = \varphi_c/\varphi_s$ ) for two different  $\varphi_s$  values (0.045 and 0.125). The values were  
491 normalized for comparison purposes. As expected, the model indicates that tile flow increases  
492 with drainable water, but the relationship is non-linear, likely because as tile carrying capacity is  
493 exceeded more frequently, there is more opportunity for groundwater seepage and  
494 evapotranspiration. The direct effect of  $\varphi_s$  (comparing the solid and dashed lines) on tile flow is  
495 small because the amount of water that can effectively drain to the tile is controlled by the  
496 capillary fringe and the associated drainable soil water. Figure 7b looks at the impact of the  
497 capillary fringe thickness on tile flow. Here, the values are also normalized. Results show that  
498  $Q_{tR}$  decreases with increasing normalized thickness of the capillary fringe,  $T_{CFR} (\frac{T_{CF}}{D_t}$ , capillary

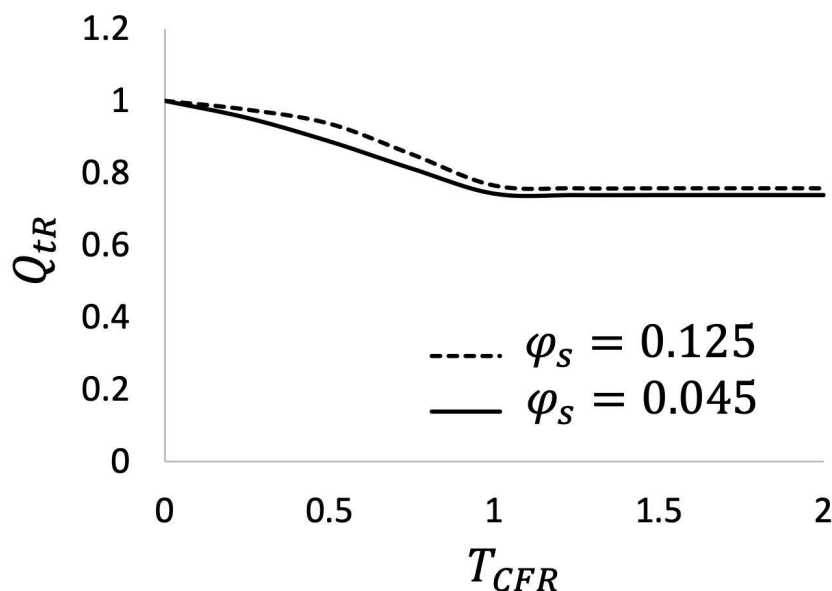


499 fringe thickness divided by tile depth), but only while the  $T_{CFR}$  is less than 1 that is when the  
500 capillary fringe position is above the tile but has not reached the soil surface. Beyond this point,  
501 increments in the capillary fringe thickness have no impact on tile flow because *Condition 1* has  
502 been reached (see Fig. 2), which essentially means that the capillary fringe has reached the soil  
503 surface.



504

505 a)



506

507 b)

508 Figure 7 Comparison between normalized tile flow ( $Q_{tR}$ ) and (a) normalized drainable soil water ( $\phi_c/\phi_s$ ) and capillary fringe  
509 thickness ( $T_{CFR}$ ) for different maximum soil saturation values ( $\phi_s$ ).

510

### 511 *Effect of capillary fringe on soil moisture*

512 Observations and model results of SWL (as an indicator of soil moisture) reveal a bimodal  
513 frequency distribution (Fig. 8 and 9, respectively) with peaks at 0.85 m and 1.25 m depth, with  
514 the former corresponding to the depth of the tile pipe and the second peak reflecting capillary  
515 fringe thickness. In the simulated SWL frequency distributions (Fig. 9), the first peak highlights  
516 again the efficiency of the tile in removing soil moisture. In contrast, the second peak indicates a  
517 strong model response to differences in the capillary fringe thickness. It shows that when there is  
518 an almost constant discharge from the bottom of the soil layer, the matric potential varies the  
519 greatest while it remains between the tile depth and the soil surface. While the matric potential



520 fluctuates faster and is more unstable within this range, it also remains there for shorter periods.

521 This bimodal response tends to push the matric potential below the tile.

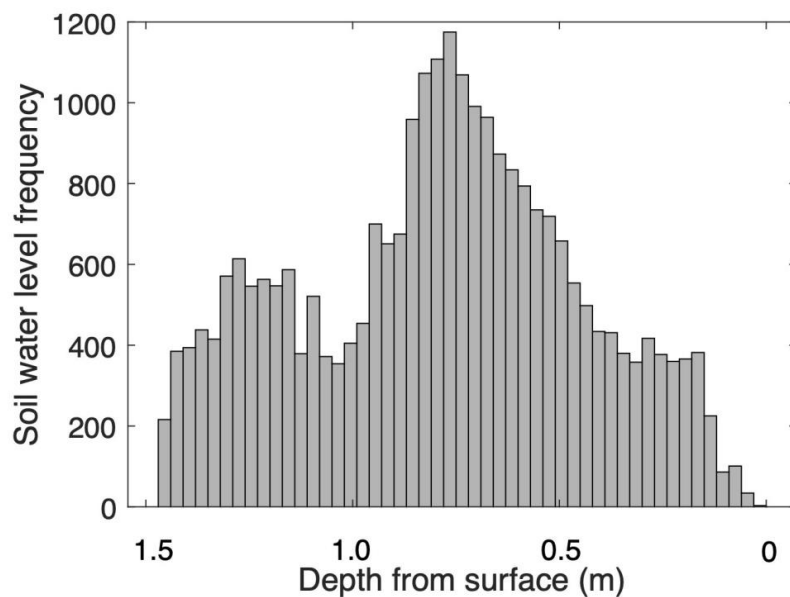
522

523 The bimodal behavior of the soil water levels demonstrated here provides the opportunity to

524 quantify the thickness of the capillary fringe using continuously monitored soil water levels. The

525 capillary fringe thickness determined using this method can then be used as an input to the TDM

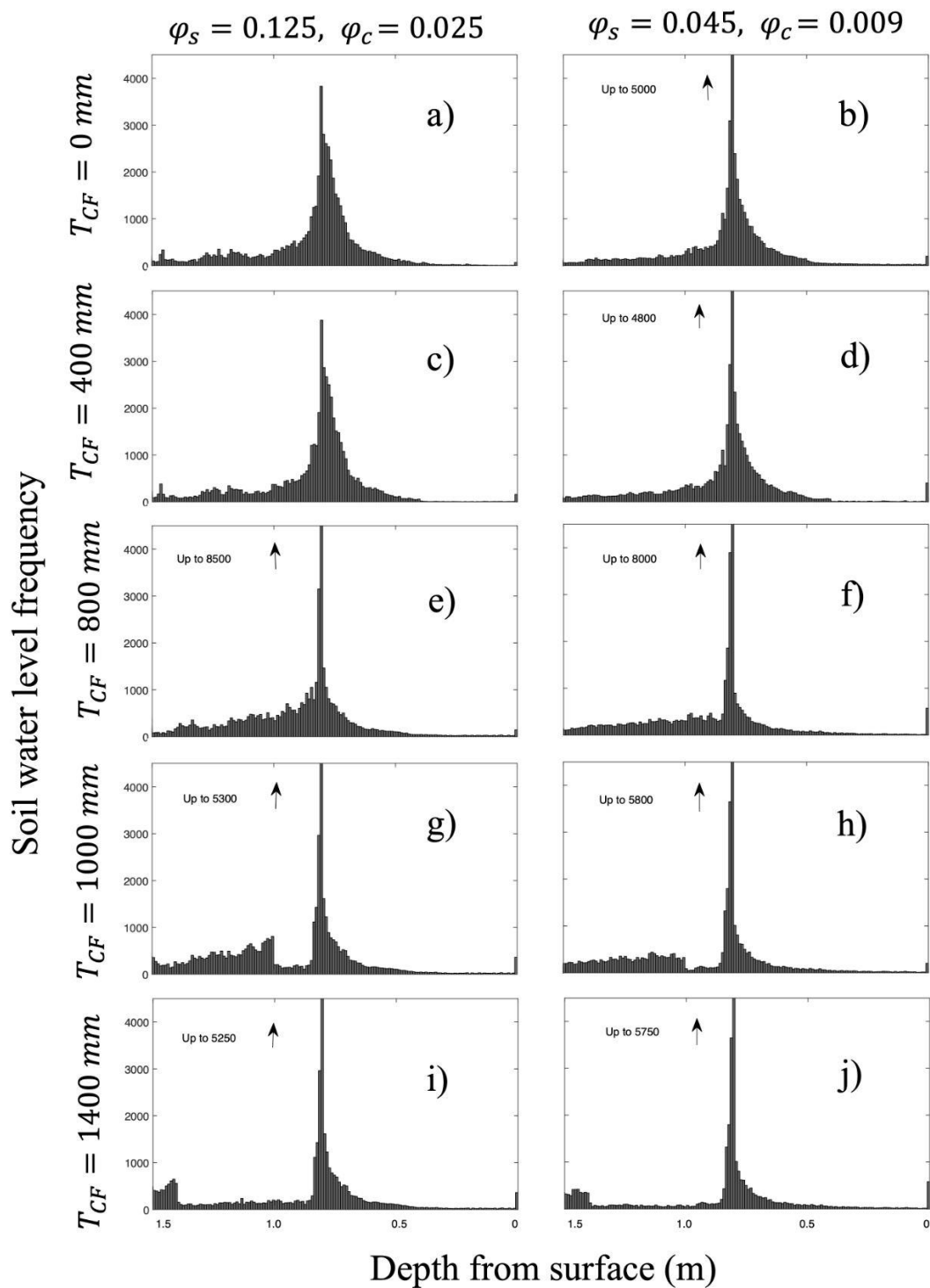
526 module.



527

528 Figure 8 Histogram of the observed soil water level distribution for the period pf 2011 to 2018 in LON.

529





531 Figure 9 Histograms of the soil water levels for the capillary fringe thicknesses of 0 (a,b), 400 (c,d), 800 (e,f), 1000 (g,h) and  
532 1400 (i, j) mm and for the  $\varphi_s$  and  $\varphi_c$  of 0.125 and 0.025 (left column) as well as 0.045 and 0.009 (right column).

533

534

## 535 **4. Discussion**

536 The new TDM module developed for CRHM was able to capture tile drainage flow and its effect  
537 on the hydrological patterns of a farm field in southern Ontario. This module can help extend the  
538 use of the CRHM platform from agricultural basins in the colder Canadian Prairies to the more  
539 temperate Great Lakes region. Tile drainage is prevalent across much of the cultivated lands in  
540 the Great Lakes basin and adjacent regions from southern Canada to the upper US Midwest. It is  
541 expanding in the eastern Canadian Prairies as well. The new TDM module will also permit  
542 simulating the impacts of a changing climate on runoff processes in these landscapes. In addition  
543 to this potential, the development of the TDM has also provided insights into hydrological  
544 processes in tile-drained landscapes. These are discussed in more detail below.

545

### 546 *4.1 Insights into key control mechanisms of tile flow for catchment-scale simulations*

547 The model suggests that tile flow may not be accurately simulated exclusively based on the  
548 matric potential and soil saturated hydraulic conductivity as suggested by the steady-state flow  
549 assumptions of the Hooghoudt's equation (Hooghoudt, 1940). Our results indicate two additional  
550 controls: (1) the amount of drainable soil water in the soil, which has also been identified in  
551 some field studies (*e.g.*, Skaggs et al., 1978; Moriasi et al., 2013) and (2) fluctuations in the  
552 groundwater table (GWRD) are equally important to account for in catchment-scale simulations.  
553 However, the relationship between drainable water and tile flow rates is non-linear, as  
554 demonstrated in Fig. 7a. This is because the opportunity time for groundwater seepage and



555 evapotranspiration increases when the hydraulic tile carrying capacity is exceeded.

556 Comparatively, the effect of soil drainable water,  $\varphi_s$  (see also Fig. 7a) on tile flow is small

557 because the capillary fringe and associated drainable soil water control the amount of water that

558 can effectively flow to the tile.

559

560 The verification of the model also indicated that the slopes of the rising and falling limbs of tile

561 flow hydrographs and SWL were very sensitive to (1) the ratio between K and drainable soil

562 water; and (2) the net outflow in the soil through tile flow and groundwater level fluctuations

563 (GWRD). This is supported by previous studies showing rapid responses of tile flow to

564 precipitation events (Gentry et al., 2007; Smith et al., 2015) and others that have related rapid

565 responses in tile discharge to antecedent moisture conditions (Macrae et al., 2007; Vidon and

566 Cuadra, 2010; Lam et al., 2016a; Macrae et al., 2019), which can be affected by the development

567 of a capillary fringe and its holding capacity.

568

569 Results show that large fluctuations in SWL and tile flow during the cold season, when the soil

570 water level tends to be above the tile, are primarily triggered by the development of the capillary

571 fringe that reduces the amount of drainable soil water. Model sensitivity tests showed that a

572 small amount of drainable soil water produces steeper rising and falling responses (and with

573 larger fluctuation amplitudes) in both the soil water level and the tile flow. Indeed, this pattern

574 can be observed by exploring differences in tile drain responses in clay loam soils with larger

575 field capacities (and correspondingly smaller drainable water) and smaller hydraulic conductivity

576 which are more likely to experience pronounced oscillations (*e.g.*, steeper rising and falling

577 response curves) compared to tile drain responses of sandy soil, which is characterized by





578 reduced capillary forces, lower field capacities (but correspondingly larger drainable water) and  
579 higher hydraulic conductivity. Notably, both model and observations of SWL (as a proxy for soil  
580 moisture) reveal a bimodal (*i.e.*, two peaks) frequency distribution when examined in relation to  
581 the tile depth and capillary fringe thickness (Fig. 8 and 9, respectively). The two peaks (*i.e.* most  
582 frequently observed SWL conditions) correspond with the (1) depth of the tile pipe (0.75 m),  
583 which demonstrates the efficacy of the tile at rapidly removing excess soil water, and the (2) the  
584 capillary fringe thickness (for the depths of 1.0 and 1.4 m, Figs. g, h, i and j) beyond which the  
585 amount of drainable water above the water level significantly increases.

586

587 These findings align well with studies such as Lam et al. (2016a) that recorded soil moisture near  
588 saturation after tile flow had ceased, suggesting the development of a capillary fringe. Combined  
589 experimental and modeling works, such as in Moriasi et al. (2013) and Logsdon et al. (2010),  
590 also discuss the impact of drainable soil water (“drainable porosity” or “specific water yield”) on  
591 tile flow and note that the drainable water is, in turn, dependent on the soil type, soil-water  
592 dynamic and soil water level depth. However, these studies did not explore the dynamic nature  
593 of the capillary fringe and its thickness relative to the soil column above in determining the  
594 transient amount of drainage soil water that will impact the SWL distribution and tile flow  
595 differently over time (*Conditions 1 to 3*, see Fig. 2). Herein, while we assumed a capillary fringe  
596 with a fixed thickness that is generally related to the soil properties, its vertical positioning was  
597 simulated dynamically, which allowed determining the drainable soil water based on the  
598 evolution of pressure head corresponding to field capacity. Thus, the development of the TDM  
599 has provided a step forward in the modeling of tile drainage at catchment scale and suggests that  
600 in loam soils such as those at the study site, the effects of a capillary fringe on tile flow should be



601 included. Soil moisture measurements from the study site by Van Esbroeck et al., (2017)  
602 between November 2011 and May 2014 from depths of 10, 30, and 50 cm (using EC-5 Soil  
603 Moisture Smart Sensor) showed that almost 90% of the gravitational soil moisture drains out  
604 with 0.5 to 2.5 h.

605

606 *4.2 Importance of capturing seasonal patterns in groundwater to improve tile flow*

607 *predictions*

608 The GWRD changed dramatically between seasons affecting soil moisture and tile flow patterns.  
609 Both observations and model results show that low precipitation and higher evapotranspiration  
610 rates tend to produce little tile flow during the growing season. These seasonal patterns in  
611 precipitation and evapotranspiration are accompanied by a reduction in soil moisture (soil water  
612 level) that leads to a substantial storage capacity in fields. Even following moderate and high-  
613 intensity storms during the growing season, rapid soil moisture increases are observed; however,  
614 tile flow rarely develops, suggesting that the soil is able to hold the water (Lam et al., 2016a;  
615 Van Esbroeck et al., 2016). In contrast, tile flow is often observed during the cold season, even  
616 during smaller rainfall-runoff and snowmelt events because of reduced soil storage but also a  
617 seasonal increase in GWRD (Lam et al., 2016a; Macrae et al., 2007, 2019; Van Esbroeck et al.,  
618 2016). This concurs with several studies throughout the Great Lakes and St. Lawrence region  
619 that have reported stronger tile responses during the non-growing season, with the summer  
620 months often showing little to no tile flow (Lam et al., 2016a, 2016b; Jamieson et al., 2003;  
621 Macrae et al., 2007; Hirt et al., 2011; King et al., 2016; Van Esbroeck et al., 2016; Plach et al.,  
622 2019).

623



624 These results (the controlling effect of soil drainable water and groundwater level fluctuations on  
625 tile flow) suggest that while soil moisture is largely controlled by tile flow rather than GWRD in  
626 the cold season, this reverses in the growing season (*i.e.* soil moisture controls tile flow), and,  
627 soil moisture is also impacted by evapotranspiration. The model indicated that the rapid drops  
628 the observed in SWL during the growing season could not be explained by evapotranspiration  
629 alone as well as the crop root depths, thus pointing at the role of GWRD.

630

## 631 **5. Conclusion**

632 A new tile drain module has been created and tested for catchment-scale simulations within the  
633 modular Cold Regions Hydrological Modelling platform to support management in agricultural  
634 basins that have seasonal snow covers. The model was tested and validated for a small working  
635 farm in southern Ontario, Canada, and presents a step forward in the dynamic simulation of tile  
636 flow and its effects on the hydrological cycle in cold climates. Observations and model results  
637 showed that the dynamic prediction of tile flow and soil moisture at catchment scales needs to  
638 account for (1) the amount of drainable soil water that can be affected by the development of a  
639 capillary fringe and (2) fluctuations in the groundwater water table, in addition to the typical (3)  
640 matric potential above the tile pipe and (4) the soil saturated hydraulic conductivity considered  
641 by the steady-state flow Hooghoudt's equation.

642

643 The groundwater table and matric potential changed dramatically between seasons, affecting  
644 patterns of soil moisture and tile flow. Observations and model results showed that low  
645 precipitation and higher evapotranspiration rates caused minimal tile flows during the crop-  
646 growing season. Conversely, tile flow was often observed during the cold season, even during



647 small rainfall-runoff and snowmelt events due to a seasonal increase in the groundwater table  
648 and soil water level.

649

650 Model sensitivity tests showed that the capillary fringe strongly affected the amount of drainable  
651 soil water flowing into the tile. Tile flow increased with drainable water, but the relationship is  
652 highly non-linear likely because, as the tile carrying capacity is exceeded more frequently, there  
653 is more opportunity time for groundwater seepage and evapotranspiration. Finally, observations  
654 and model results reveal a bimodal soil moisture response in the presence of tiles, which is  
655 controlled by the relative positioning of the capillary fringe in relation to the soil surface and tile  
656 pipe. Capturing these dynamics is a critical advance enabling the accurate prediction of the swift  
657 hydrological changes caused by the presence of tiles in catchment-scale models.

658

659

#### 660 **Author contribution**

661 MK and DC developed the model code and performed the simulations. MM prepared the data  
662 and supported the field work. MK and DC prepared the manuscript with contribution of MM, JP  
663 and RP.

664

#### 665 **Acknowledgements**

666 Funding for this project was provided by the Canada First Excellence Research Fund's Global  
667 Water Futures programme through its Agricultural Water Futures project. Funding for the  
668 collection of the field data was provided by the Ontario Ministry of Agriculture, Food and Rural



669 Affairs. The support of Biogeochemistry Lab at the University of Waterloo for the collection of  
670 field data and of Tom Brown and Xing Fang of the Centre for Hydrology at the University of  
671 Saskatchewan for CRHM development and updates is gratefully acknowledged. The Maitland  
672 Valley Conservation Authority is thanked for providing some precipitation, rainfall and  
673 temperature data.

674

## 675 **References**

676 Arheimer, B., Nilsson, J., and Lindstrom, G.: Experimenting with Coupled Hydro-Ecological  
677 Models to Explore Measure Plans and Water Quality Goals in a Semi-Enclosed Swedish Bay,  
678 *Water*, 7(7), 3906-3924, <https://doi.org/10.3390/w7073906>, 2015.

679

680 Arnold, J. G., Srinivasan, R., Muttiah, R. S., and Williams, J. R.: Large area hydrologic  
681 modeling and assessment part I: model development, *J. Am. Water. Resour. Assoc.*, 34, 73-89,  
682 <https://doi.org/10.1111/j.1752-1688.1998.tb05961.x>, 1998.

683

684 Badr, A. W.: Physical properties of some North Carolina Organic Soils and the effect of land  
685 development on these properties, M.S. Thesis, Department of Biological and Agricultural  
686 Engineering, North Carolina State University, Raleigh, NC. 67 p., 1978.

687

688 Blears, W. (2<sup>nd</sup> Edition): *Soil and Environmental Chemistry*, Academic Press, eBook ISBN:  
689 9780128041956, 2017.

690



- 691 Bouwer, H. and van Schilfgaarde, J.: Simplified method of predicting the fall of water table in  
692 drained land, *Trans. ASAE*. 6(4), 288-291, 296, 1963.
- 693
- 694 Brockley, R. P.: The effect of nutrient and moisture on soil nutrient availability, nutrient uptake,  
695 tissue nutrient concentration, and growth of Douglas-Fir seedlings, Master Thesis, The  
696 University of British Columbia, 1976.
- 697
- 698 Broughton, R. and Jutras, P.: Farm Drainage. In the Canadian Encyclopedia,  
699 <https://www.thecanadianencyclopedia.ca/en/article/farm-drainage/>, last access: 14 February  
700 2019.
- 701
- 702 Coelho, B. B., Murray, R., Lapen, D., Topp, E., and Bruin, A.: Phosphorus and sediment loading  
703 to surface waters from liquid swine manure application under different drainage and tillage  
704 practices, *Agric. Water Manag.*, 104, 51-61, <https://doi.org/10.1016/j.agwat.2011.10.020>, 2012.
- 705
- 706 Cordeiro, M. R. C. and Ranjan, R. S.: Corn yield response to drainage and subirrigation in the  
707 Canadian Prairies, *Trans. ASABE*. 55(5), 1771-1780, <https://doi.org/10.13031/2013.42369>,  
708 2012.
- 709
- 710 Cordeiro, M. R. C., Wilson, H. F., Vanrobaeys, J., Pomeroy, J. W., Fang, X., and The Red-  
711 Assiniboine Project Biophysical Modeling Team: Simulating cold-region hydrology in an  
712 intensively drained agricultural watershed in Manitoba, Canada, using the Cold Region



713 Hydrological Model, Hydrol. Earth Syst. Sci., 21, 3483-3506, <https://doi.org/10.5194/hess-21->  
714 [3483-2017](https://doi.org/10.5194/hess-21-3483-2017), 2017.

715

716 Correll, D.: The role of phosphorus in the eutrophication of receiving waters: a review, J.  
717 Environ. Qual., 27, 261-266, <https://doi.org/10.2134/jeq1998.00472425002700020004x>, 1998.

718

719 Costa, D., Baulch, H., Elliott, J., Pomeroy, J., and Wheater, H.: Modelling nutrient dynamics in  
720 cold agricultural catchments: A review, Environ. Model. Softw., 124, 104586,  
721 <https://doi.org/10.1016/j.envsoft.2019.104586>, 2020a.

722

723 Costa, D., Shook, K., Spence, C., Elliott, J., Baulch, H., Wilson, H., and Pomeroy, J.: Predicting  
724 variable contributing areas, hydrological connectivity, and solute transport pathways for a  
725 Canadian Prairie basin, Water Resour. Res., 56, 1-23, <https://doi.org/10.1029/2020WR02798>,  
726 2020b.

727

728 Costa, D., Pomeroy, J. W., Brown, T., Baulch, H., Elliott, J., and Macrae, M.: Advances in the  
729 simulation of nutrient dynamics in cold climate agricultural basins: Developing new nitrogen and  
730 phosphorus modules for the Cold Regions Hydrological Modelling Platform, J. Hydrol., 603, 1-  
731 17, <https://doi.org/10.1016/j.jhydrol.2021.126901>, 2021.

732

733 De Ridder, N. A., Takes, C. A. P., van Someren, C. L., Bos, M. G., Messemaeckers van de  
734 Graaff, R. H., Bokkers, A. H. J., Stransky, J., Wiersma-Roche, M. F. L., and Beekman, T.:



735 Drainage Principles and Applications. International Institute for Lan Reclamation and  
736 Improvement, P.O. Box 45 Wageningen The Netherlands, 1974.  
737  
738 Du, B., Arnold, J. G., Saleh, A., and Jaynes, D. B.: Development and application of SWAT to  
739 landscapes with tiles and potholes, Trans. ASAE, 48, 1121-1133,  
740 <https://doi.org/10.13031/2013.18522>, 2005.  
741  
742 Du, B., Saleh, A., Jaynes, D. B., and Arnold, J. G.: Evaluation of SWAT in simulating nitrate  
743 nitrogen and atrazine fates in a watershed with tiles and potholes, Trans. ASABE, 49, 949-959,  
744 <https://doi.org/10.13031/2013.21746>, 2006.  
745  
746 ECCC, Canadian Climate Normals 1981-2010 Station Data,  
747 [https://climate.weather.gc.ca/climate\\_normals/results\\_1981\\_2010\\_e.html?searchType=stnProx&txtRadius=25&selCity=&selPark=&optProxType=custom&txtCentralLatDeg=43&txtCentralLatMin=41&txtCentralLatSec=55&txtCentralLongDeg=81&txtCentralLongMin=28&txtCentralLongSec=47&txtLatDecDeg=&txtLongDecDeg=&stnID=4545&dispBack=0](https://climate.weather.gc.ca/climate_normals/results_1981_2010_e.html?searchType=stnProx&txtRadius=25&selCity=&selPark=&optProxType=custom&txtCentralLatDeg=43&txtCentralLatMin=41&txtCentralLatSec=55&txtCentralLongDeg=81&txtCentralLongMin=28&txtCentralLongSec=47&txtLatDecDeg=&txtLongDecDeg=&stnID=4545&dispBack=0), last access: 5  
750 February 2020.  
751  
752  
753 Eckersten, H., Jansson, P. -E., and Johnsson, H. (2<sup>nd</sup> edition): SOILN model-user's manual,  
754 Division of Agricultural Hydrotechnics Communications 94:4, Department of soil Sciences,  
755 Swedish University of Agricultural Sciences, 58pp, Uppsala, 1994.  
756





757 Environment Canada, Canadian Climate Normals 1981-2010 Station Data,  
758 [https://climate.weather.gc.ca/climate\\_data/daily\\_data\\_e.html?hlyRange=%7C&dlyRange=1966-06-01%7C2021-06-14&mlyRange=1966-01-01%7C2006-12-01&StationID=4603&Prov=ON&urlExtension=\\_e.html&searchType=stnName&optLimit=yearRange&StartYear=1840&EndYear=2022&selRowPerPage=25&Line=0&searchMethod=contains&Month=6&Day=4&txtStationName=Wroxeter&timeframe=2&Year=2021](https://climate.weather.gc.ca/climate_data/daily_data_e.html?hlyRange=%7C&dlyRange=1966-06-01%7C2021-06-14&mlyRange=1966-01-01%7C2006-12-01&StationID=4603&Prov=ON&urlExtension=_e.html&searchType=stnName&optLimit=yearRange&StartYear=1840&EndYear=2022&selRowPerPage=25&Line=0&searchMethod=contains&Month=6&Day=4&txtStationName=Wroxeter&timeframe=2&Year=2021), last access: 10  
763 May 2020.  
764  
765 Fang, X., Pomeroy, J. W., Westbrook, C. J., Guo, X., Minke, A. G., and Brown, T.: Prediction of  
766 snowmelt derived streamflow in a wetland dominated prairie basin, Hydrol. Earth Syst. Sci., 14,  
767 991-1006, <https://doi.org/10.5194/hess-14-991-2010>, 2010.  
768  
769 Fang, X., Pomeroy, J. W., Ellis, C. R., MacDonald, M. K., DeBeer, C. M., and Brown, T.: Multi-  
770 variable evaluation of hydrological model predictions for a headwater basin in the Canadian  
771 Rocky Mountains, Hydrol. Earth Syst. Sci., 17, 1635-1659, <https://doi.org/10.5194/hess-17-1635-2013>, 2013.  
772  
773  
774 Filippelli, G. M.: The global phosphorus cycle, Rev. Mineral. and Geochem., 48, 391-425,  
775 <https://doi.org/10.2138/rmg.2002.48.10>, 2002.  
776  
777 Frey, S. K., Hwang, H. T., Park, Y. J., Hussain, S. I., Gottschall, N., Edwards, M., and Lapen, D.  
778 R.: Dual permeability modeling of tile drain management influences on hydrologic and nutrient



779 transport characteristics in macroporous soil, J. Hydrol., 535, 392-406,  
780 <https://dx.doi.org/10.1016/j.jhydrol.2016.01.073>, 2016.  
781  
782 Gentry, L. E., David, M. B., Royer, T. V., Mitchell, C. A., and Starks, K.: Phosphorus transport  
783 pathways to streams in tile-drained agricultural watersheds, J. Environ. Quality., 36, 408-415,  
784 <https://doi.org/10.2134/jeq2006.0098>, 2007.  
785  
786 Garcia-Gutierrez, C., Pachepsky, Y., and Martin, M. A.: Technical note: Saturated hydraulic  
787 conductivity and textural heterogeneity of soils, Hydrol. Earth Syst. Sci., 22, 3923-3932,  
788 <https://doi.org/10.5194/hess-22-3923-2018>, 2018.  
789  
790 Green, C. H., Tomer, M. D., Di Luzio, M., and Arnold, J. G.: Hydrologic evaluation of the Soil  
791 and Water Assessment Tool for large tile-drained watershed in Iowa, Trans. ASABE., 49, 413-  
792 422, <https://doi.org/10.13031/2013.20415>, 2006.  
793  
794 Hirt, U., Wetzig, A., Amatya, M. D., and Matranga, M.: Impact of seasonality on artificial  
795 drainage discharge under temperate climate conditions, Int. Rev. Hydrobiol., 96, 561-577,  
796 <https://doi.org/10.1002/iroh.201111274>, 2011.  
797  
798 Hooghoudt, S. B.: Bijdrage tot de kennis van enige natuurkundige grootheden van de grond.  
799 Verslagen van Landbouwkundige Onderzoekingen, 46(7), 515-707, the Hague, The Netherlands  
800 (in Dutch), 1940.  
801



802 ICID: World Drained Area-2018. International Commission on Irrigation and Drainage.  
803 <http://www.icid.org/world-drained-area.pdf> , last access: 14 February 2019.  
804  
805 Jamieson, A., Madramootoo, C. A., and Enright, P.: Phosphorus losses in surface and subsurface  
806 runoff from a snowmelt event on an agricultural field in Quebec, Can. Biosyst. Eng., 45, 11-17,  
807 2003.  
808  
809 Jarvie, H. P., Johnson, L. T., Sharpley, A. N., Smith, D. R., Baker, D. B., Bruulsema, T. W., and  
810 Confesor, R.: Increased Soluble Phosphorus Loads to Lake Erie: Unintended Consequences of  
811 Conservation Practices?, J. Environ. Qual., 46, 123-132,  
812 <https://doi.org/10.2134/jeq2016.07.0248>, 2017.  
813  
814 Javani-Jouni, H., Liaghat, A., Hassanoghli, A., and Henk, R.: Managing controlled drainage in  
815 irrigated farmers' fields: A case study in the Moghan Plain, Iran, Agric. Water Manag., 208, 393-  
816 405, <https://doi.org/10.1016/j.agwat.2018.06.037>, 2018.  
817  
818 Kiesel, J., Fohrer, N., Schmalz, B., and White, M. J.: Incorporating landscape depressions and  
819 tile drainages of a northern German lowland catchment into a semi-distributed model, Hydrol.  
820 Process., 24, 1472-1486, <https://doi.org/10.1002/hyp.7607>, 2010.  
821  
822 King, K. W., Williams, M. R., Macrae, M. L., Fausey, N. R., Frankenberger, J., Smith, D. R.,  
823 Kleinman, P. A. J., and Brown, L. C.: Phosphorus transport in agricultural subsurface drainage:  
824 A review, J. Environ. Qual., 44(2), 467-485, <https://doi.org/10.2134/jeq2014.04.0163>, 2015.



825

826 King, K. W., Williams, M. R., and Fausey, N. R.: Effect of crop type and season on nutrient  
827 leaching to tile drainage under a corn-soybean rotation, *J. Soil and Water Conserv.*, 71, 56-68,  
828 <https://doi.org/10.2489/jswc.71.1.56>, 2016.

829

830 Kirkham, D.: Theory of land drainage, in, *Drainage of Agricultural Lands*. Agronomy  
831 Monograph, No. 7, American Society of Agronomy, Madison, Wisconsin, 1957.

832

833 Kladvik, E. J., Grochulska, J., Turco, R. F., Van Scoyoc, G. E., and Eigel, J. D.: Pesticide and  
834 nitrate transport into subsurface tile drains of different spacings, *J. Environ. Qual.*, 28, 997-1004,  
835 <https://doi.org/10.2134/jeq1999.00472425002800030033x>, 1999.

836

837 Klaiber, L. B., Kramer, S. R., and Young, E. O.: Impacts of Tile Drainage on Phosphorus Losses  
838 from Edge-of-field Plots in the Lake Champlain Basin of New York, *Water*, 12, 328,  
839 <https://doi.org/10.3390/w12020328>, 2020.

840

841 Kock, S., Bauwe, A., and Lennartz, B.: Application of SWAT Model for a Tile-Drained Lowland  
842 Catchment in North-Eastern Germany on Subbasin Scale, *Water Resour. Manage.*, 27, 791-805,  
843 <https://doi.org/10.1007/s11269-012-0215-x>, 2013.

844

845 Kokulan, V.: Environmental and Economic Consequences of Tile Drainage Systems in Canada,  
846 The Canadian Agri-Food Policy Institute (CAPI), 2019.

847



848 Kokulan, V., Macrae, M. L., Ali, G. A., and Lobb, D. A.: Hydroclimatic controls on runoff  
849 activation in a artificially drained, near-level vertisolic clay landscape in a Prairie climate, *Hyrol.*  
850 *Process.*, 33, 602-615, <https://doi.org/10.1002/hyp.13347>, 2019a.  
851  
852 Lam, W. V., Macrae, M. L., English, M. C., O'Halloran, I. P., Plach, J. M., and Wang, Y.:  
853 Seasonal and event-based drives of runoff and phosphorus export through agricultural tile drains  
854 under sandy loam soil in a cool temperate region, *Hydro. Process.*, 30, 2644-2656,  
855 <https://doi.org/10.1002/hyp.10871>, 2016a.  
856  
857 Lam, W. V., Macrae, M. L., English, M. C., O'Halloran, I., and Wang, Y.: Effects of tillage  
858 practices on phosphorus transport in tile drain effluent in sandy loam agricultural soils in  
859 Ontario, Canada, *J. Great Lakes Res.*, 42(6), 1260-1270,  
860 <https://dx.doi.org/10.1016/j.jglr.2015.12.015>, 2016b.  
861  
862 Larsbo, M., and Jarvis, N.: MACRO 5.0. A model of water flow and solute transport in  
863 microporous soil, Technical description. Swedish University of Agricultural Sciences, Division  
864 of Environmental Physics, Emergo 2003:6 Report, ISSN 1651-7210, ISBN 91-576-6592-3,  
865 2003.  
866  
867 Lindstrom, G., Pers, C., Rosberg, J., Stromqvist, J., and Arheimer, B.: Development and testing  
868 of the HYPE (Hydrological Predictions for the Environment) water quality model for different  
869 scales, *Hydro. Res.*, 41(3-4), 295-319, <https://doi.org/10.2166/nh.2010.007>, 2010.  
870



871 Logsdon, S. D., Schilling, K. E., Hernandez-Ramirez, G., Prueger, J. H., Hatfield, J. L., and  
872 Sauer, T. J.: Field estimation of specific yield in a central Iowa crop field, *Hydrol. Process.*, 24,  
873 1369-1377, <https://doi.org/10.1002/hyp.7600>, 2010.  
874  
875 Macrae, M. L., English, M. C., Schiff, S. L., and Stone, M. L.: Intra-annual variability in the  
876 contribution of tile drains to basin discharge and phosphorus export in a first order agricultural  
877 catchment, *Agric. Water Manag.*, 92, 171-182, <https://doi.org/10.1016/j.agwat.2007.05.015>,  
878 2007.  
879  
880 Macrae, M. L., Ali, G. A., King, K. W., Plach, J. M., Pfluer, W. T., Williams, M., Morison, M.  
881 Q., and Tang, W.: Evaluating Hydrologic Response in Tile-Drained Landscapes: Implications for  
882 Phosphorus Transport, *J. Environ. Qual.*, 48(5), 1347-1355,  
883 <https://doi.org/10.2134/jeq2019.02.0060>, 2019.  
884  
885 Malzone, J. M., Lowry, C. S., and Ward, A. S.: Response of the hyporheic zone to transient  
886 groundwater fluctuations on the annual and storm event time scales, *Water Resour. Res.*, 52,  
887 5301-5321, <https://doi.org/10.1002/2015WR018056>, 2016.  
888  
889 Moriasi, D. N., Arnold, J. G., Van Liew, M. W., Bingner, R. L., Harmel, R. D., and Veith, T. L.:  
890 Model Evaluation Guidelines for Systematic Quantification of Accuracy in Watershed  
891 Simulations, *Trans. ASABE*, 50(3), 885-900, <https://doi.org/10.13031/2013.23153>, 2007.  
892



893 Moriasi, D. N., Gowda, P. H., Arnold, J. G., Mulla, D. J., Ale, S., Steiner, J. L., and Tomer, M.  
894 D.: Evaluation of the Hooghoudt and Kirkham Tile Drain Equations in the Soil and Water  
895 Assessment Tool to Simulate Tile Flow and Nitrate-Nitrogen, *J. Environ. Qual.*, 42, 1699-1710,  
896 <https://doi.org/10.2134/jeq2013.01.0018>, 2013.  
897  
898 Plach, J. M., Macrae, M. L., Ali, G. A., Brunke, R. R., English, M. C., Ferguson, G., Lam, W.  
899 V., Lozier, T. M., McKague, K., O'Halloran, I. P., Opolko, G., and Van Esbroeck, C. J.: Supply  
900 and Transport Limitations on Phosphorus Losses from Agricultural Fields in the Lower Great  
901 Lakes Region, Canada, *J. Environ. Qual.*, 47, 96-105, <https://doi.org/10.2134/jeq2017.06.0234>,  
902 2018a.  
903  
904 Plach, J. M., Macrae, M. L., Williams, M. R., Lee, B. D., and King, K. W.: Dominant glacial  
905 landforms of the lower Great Lakes region exhibit different soil phosphorus chemistry and  
906 potential risk for phosphorus loss, *J. Great Lakes Res.*, 44, 1057-1067,  
907 <https://doi.org/10.1016/j.jglr.2018.07.005>, 2018b.  
908  
909 Plach, J., Pluer, W., Macrae, M., Kompanizare, M., McKague, K., Carlow, R., and Brunke, R.:  
910 Agricultural Edge of Field Phosphorus Losses in Ontario, Canada: Importance of the  
911 Nongrowing Season in Cold Regions, *J. Environ. Qual.*, 48, 813-821,  
912 <https://doi.org/10.2134/jeq2018.11.0418>, 2019.  
913



914 Pluer, W. T., Macrae, M., Buckley, A., and Reid, K.: Contribution of preferential flow to tile  
915 drainage varies spatially and temporally, *Vadose Zone J.*, 19: e20043,  
916 <https://doi.org/10.1002/vzj2.20043>, 2020.

917

918 Pomeroy, J. W., Gray, D. M., Shook, K. R., Toth, B., Essery, R. L. H., Pietroniro, A., and  
919 Hedstrom, N. R.: An evaluation of snow accumulation and ablation processes for land surface  
920 modelling, *Hydrol. Process.*, 12, 2339-2367, [https://doi.org/10.1002/\(SICI\)1099-  
921 1085\(199812\)12:15](https://doi.org/10.1002/(SICI)1099-1085(199812)12:15), 1998.

922

923 Pomeroy, J. W., Gray, D. M., Brown, T., Hedstrom, N. R., Quinton, W. L., Granger, R. J., and  
924 Carey, S. K.: The cold regions hydrological model: a platform for basing process representation  
925 and model structure on physical evidence, *Hydrol. Process.*, 21, 2650-2667,  
926 <https://doi.org/10.1002/hyp.6787>, 2007.

927

928 Pomeroy, J. W., Fang, X., Shook, K., and Whitfield, P. H.: Predicting in Ungauged Basins Using  
929 Physical Principles Obtained Using the Deductive, Inductive, and Abductive Reasoning  
930 Approach, [https://research-  
931 groups.usask.ca/hydrology/documents/pubs/papers/pomeroy\\_et\\_al\\_2003\\_3.pdf](https://research-groups.usask.ca/hydrology/documents/pubs/papers/pomeroy_et_al_2003_3.pdf), 2013.

932

933 Pomeroy, J. W., Fang, X., and Marks, D. G.: The cold rain-on-snow event of June 2013 in the  
934 Canadian Rockies - characteristics and diagnosis, *Hydrol. Process.*, 30, 2899-2914,  
935 <https://doi.org/10.1002/hyp.10905>, 2016.

936





- 937 Pomeroy, J. W., Brown, T., Fang, X., Shook, K. R., Pradhananga, D., Armstrong, R., Harder, P.,  
938 Marsh, C., Costa, D., Krogh, S. A., Aubry-Wake, C., Annand, H., Lawford, P., He, Z.,  
939 Kompanizare, M., and Lopez Moreno, J. I.: The cold regions hydrological modelling platform  
940 for hydrological diagnosis and prediction based on process understanding, *J. of Hydrol.*, 615 (A),  
941 128711, <https://doi.org/10.1016/j.jhydrol.2022.128711>, 2022.  
942  
943 Qi, P., Zhang, G., Xu, Y. J., Wang, L., Ding, C., and Cheng, C.: Assessing the Influence of  
944 Precipitation on Shallow Groundwater Table Response Using Combination of Singular Value  
945 Decomposition and Cross-Wavelet Approaches, *Water*, 10, 598,  
946 <https://doi.org/10.3390/w10050598>, 2018.  
947  
948 Quinton, J. G., Govers, G., van Oost, K., and Bardgett, R.: The impact of agricultural soil erosion  
949 on biochemical cycling, *Nat. Geosci.*, 3, 311-314, <https://doi.org/10.1038/ngeo838>, 2010.  
950  
951 Raats, P. A. C. and Gardner, W. R.: Movement of water in saturated zone near a water table. Ch.  
952 13 in *Drainage for agriculture*, J. van Schilfgraade, Ed., *Agronomy Monograph*. No. 17,  
953 American Society of Agronomy, Madison, WI, pp. 331-357, 1974.  
954  
955 Radcliffe, D. E., Reid, D. K., Blomback, K., Bolster, C. H., Collick, A. S., Easton, Z. M.,  
956 Francesconi, W., Fuka, D. R., Johnsson, H., King, K., Larsbo, M., Youssef, M. A., Mulkey, A.  
957 S., Nelson, N. O., Persson, K., Ramirez-Avila, J. J., Schmieder, F., and Smith, D. R.:  
958 Applicability of Models to Predict Phosphorus Losses in Drained Fields: A Review, *J. Environ.*  
959 *Qual.*, 44, 614-628, <https://doi.org/10.2134/jeq2014.05.0220>, 2015.



960

961 Rahman, M. M., Lin, Z., Jia, X., Steele, D. D., and DeSutter, T. M.: Impact of subsurface

962 drainage on streamflows in Red River of the North basin, *J. Hydrol.*, 511, 474-483,

963 <https://doi.org/10.1016/j.jhydrol.2014.01.070>, 2014.

964

965 Refsgaard, J. C. and Storm, B.: MIKE SHE. In: Singh VP (ed) Computer models of watershed

966 hydrology, Highlands Ranch, Water Research Pub, Colorado, 1995.

967

968 Richards L. A.: Capillary conduction of liquids through porous medium, *Physics*, 1 (5): 318-333,

969 Bibcode:1931Physi...1..318R. <https://doi.org/10.1063/1.1745010>, 1931.

970

971 Rozemeijer, J. C., Visser, A., Borren, W., Winegram, M., van der Velde, Y., Klein, J., and

972 Broers, H. P.: High-frequency monitoring of water fluxes and nutrient loads to assess the effects

973 of controlled drainage on water storage and nutrient transport, *Hydrol. Earth Syst. Sci.*, 20, 347-

974 358, <https://doi.org/10.5194/hess-20-347-2016>, 2016.

975

976 Rust, W., Holman, I., Bloomfield, J. Cuthbert, M., and Corstanje, R.: Understanding the potential

977 of climate teleconnections to project future groundwater drought, *Hydrol. Earth Syst. Sci.*, 23,

978 3233-3245, <https://doi.org/10.5194/hess-23-3233-2019>, 2019.

979

980 Ruttenger, K.: The global phosphorus cycle. In *Biochemistry*, Vol. 8, treatise on geochemistry,

981 Schlesinger W (ed) (eds. H. Holland and K. Turekian). Elsevier-Pergamon: Oxford; 585-643,

982 2005.



983

984 Searcy, J. and Hardison, C. H.: Double –Mass Curves. Manual of Hydrology: Part 1, General  
985 Surface-Water Techniques, Geological Survey Water-Supply Paper 1541-B, 1960.

986

987 Schindler, D. W.: Recent advances in the understanding and management of eutrophication,  
988 Limnol. Oceanogr., 51, 356-363, [https://doi.org/10.4319/lo.2006.51.1\\_part\\_2.0356](https://doi.org/10.4319/lo.2006.51.1_part_2.0356), 2006.

989

990 Sharpley, A. N., Hedley, M. J., Sibbesen, E., Hillbricht-Ilkowska, A., House, W. A., and  
991 Ryszkowski, L.: Phosphorus transfer from terrestrial to aquatic ecosystems, In Phosphorus in the  
992 global environment, Tiessen H (ed), Scientific Committee on Problems of the Environment  
993 (SCOPE). John Wiley & SonsLtd.: Chichester; 171-199, 1995.

994

995 Simunek J., van Genuchten M. Th., and Sejna M.: The HYDRUS Software Package for  
996 Simulating Two- and Three-Dimensional Movement of Water, Heat and Multiple Solutes in  
997 Variably-Saturated Media, Technical Manual, Version 2.0, PC Progress, Prague, Czech  
998 Republic, pp. 258, 2011.

999

1000 Skaggs, R. W.: A water management model for shallow water table soils, University of North  
1001 Carolina, Water Resource Research Institute, Technical Report 134, 1978.

1002

1003 Skaggs, R. W.: Combination surface-subsurface drainage systems for humid regions. J. Irrig.  
1004 Drain. Div., ASCE. 106(IR4), 265-283, 1980a.

1005



- 1006 Skaggs, R. W.: Drainmod Reference Report, Methods for Design and Evaluation of Drainage-  
1007 Water Management Systems for Soils with High Water Tables, U.S. Department of Agriculture,  
1008 Soil Conservation Service, North Carolina State University, Raleigh, North Carolina, 1980b.  
1009
- 1010 Skaggs, R. W., Wells, L. G., and Ghatge, S. R.: Predicted and measured drainable porosities for  
1011 field soils, Trans. ASAE, 21(3), 522-528, [https://uknowledge.uky.edu/bae\\_facpub/199](https://uknowledge.uky.edu/bae_facpub/199), 1978.  
1012
- 1013 Skaggs, R. W., Youssef, M. A., and Chescheir, G. M.: DRAINMOD: Model Use, Calibration,  
1014 and Validation, Trans. ASABE, 55(4), 1509-1522, <https://doi.org/10.13031/2013.42259>, 2012.  
1015
- 1016 Smedema, L. K., Vlotman, W. F., and Rycroft, D.: Modern land Drainage. Planning, design and  
1017 management of agricultural drainage systems, London: Taylor & Francis.  
1018 <https://doi.org/10.1201/9781003>, 2004.  
1019
- 1020 Smith, D. R., King, K. W., Johnson, L., Francesconi, W., Richards, P., Baker, D., and Sharpley,  
1021 A. N.: Surface runoff and tile drainage transport of phosphorus in the Midwestern United States,  
1022 J. Environ. Qual., 44, 495-502, <https://doi.org/10.2134/jeq2014.04.0176>, 2015.  
1023
- 1024 Tomer, M. D., Meek, D. W., Jaynes, D. B., and Hatfield, J. L.: Evaluation of nitrate nitrogen  
1025 fluxes from a tile-drained watershed in Central Iowa, J. Environ. Qual., 32, 642-653,  
1026 <https://doi.org/10.2134/jeq2003.6420>, 2003.  
1027



- 1028 Twarakavi, N. K. C., Sakai, M., and Simunek, J.: An objective analysis of the dynamic nature of  
1029 field capacity, *Water Resour. Res.*, 45, W10410, <https://doi.org/10.1029/2009WR007944>, 2009.  
1030
- 1031 Van Esbroeck, C. J., Macrae, M. L., Brunke, R. I., and McKague, K.: Annual and seasonal  
1032 phosphorus export in surface runoff and tile drainage from agricultural fields with cold temperate  
1033 climates, *J. Great Lakes Res.*, 42(6), 1271-1280, <https://doi.org/10.1016/j.jglr.2015.12.014>, 2016.  
1034
- 1035 Van Esbroeck, C. J., Macrae, M. L., Brunke, R. R., and McKague, K.: Surface and subsurface  
1036 phosphorus export from agricultural fields during peak flow events over the nongrowing season  
1037 in regions with cool, temperate climates, *Journal of Soil and Water Conservation*, 72(1), 65-76,  
1038 <https://doi:10.2489/jswc.72.1.65>, 2017.  
1039
- 1040 Van Schilfgaarde, J.: Nonsteady flow to drains, In *Drainage for Agriculture*, J. van Schilfgaarde,  
1041 ed. American Society of Agronomy, Madison, WI. PP 245-270, 1974.  
1042
- 1043 Vidon, P. and Cuadra, P. E.: Impact of precipitation characteristics on soil hydrology in tile  
1044 drained landscapes, *Hydrol. Process.*, 24, 1821-1833, <https://doi.org/10.1002/hyp.7627>, 2010.  
1045
- 1046 Vivekananthan, K.: Environmental and Economic Consequences of Tile Drainage Systems in  
1047 Canada, The Canadian Agri-Food Policy Institute, [www.capi-icpa.ca](http://www.capi-icpa.ca), 2019.  
1048



1049 Vivekananthan, K., Macrae, M., Lobb, D. A., and Ali, G. A.: Contribution of overland and tile  
1050 flow to runoff and nutrient losses from vertisols in Manitoba, Canada, *J. Environ. Qual.*, 48(4),  
1051 959-965, <https://doi.org/10.2134/jeq2019.03.0103>, 2019.

1052

1053 Waichler, S. R. and Wigmosta, M. S.: Development of Hourly Meteorological Values from  
1054 Daily Data and Significance to Hydrological Modeling at H. J. Andrews Experimental Forest,  
1055 *Am. Meteorol. Soc.*, 4, 251-263, [https://doi.org/10.1175/1525-  
1056 7541\(2003\)4<251:DOHMFV>2.0.CO;2](https://doi.org/10.1175/1525-7541(2003)4<251:DOHMFV>2.0.CO;2), 2003.

1057

1058 Williams, M. R., King, K. W., and Fausey, N. R.: Drainage water management effects on tile  
1059 discharge and water quality, *Agric. Water Manag.*, 148, 43-51,  
1060 <http://dx.doi.org/10.1016/j.agwat.2014.09.017>, 2015.

1061

1062 Williams, M. R., King, K. W., Ford, W., Buda, A. R., and Kennedy, C. D.: Effect of tillage on  
1063 macropore flow and phosphorus transport to tile drains, *Water Resour. Res.*, 52, 2868-2882,  
1064 <https://doi.org/10.1002/2015WR017650>, 2016.

1065

1066 Williams, M. R., Livingston, S. J., Heathman, G. C., and McAfee, S. J.: Thresholds for run-off  
1067 generation in a drained closed depression, *Hydrol. Process.*, 1-14,  
1068 <https://doi.org/10.1002/hyp.13477>, 2019.

1069



1070 Youngs, E. G.: Effect of the Capillary fringe on Steady-State Water Tables in drained Lands, J.

1071 Irrig. Drain. Eng., 138(9), 809-814, [https://doi.org/10.1061/\(ASCE\)IR.1943-4774.0000467](https://doi.org/10.1061/(ASCE)IR.1943-4774.0000467),

1072 2012.

1073

1074

1075 **Appendix A**

1076 Table A1 Instrument names and descriptions

Instrument name	Description
Hach Flo-tote and FL900 logger	Flow velocity and water level measurement
U20, Onset Ltd.	Barometrically-corrected pressure transducer
Temperature Smart Sensor S-THB-M002	Air temperature measurement
Wind Smart Sensor S-WSET-M002	Wind speed measurement
(Silicon Pyranometer)-S-LIB-M003	Solar radiation sensor
Tipping bucketrain gauge, 0.2 mm Rainfall Smart Sensor – SRGB-M002	Rainfall measurement
RH Smart Sensor(S-THB-M002)	Relative Humidity measurement

1077

1078

1079

1080 **Appendix B**

1081 Table B1 Parameter names and their symbols in CRHM platform

Parameter symbol	Parameter name
Tair	Air temperature



Wspeed	Wind speed
RH	Relative Humidity
Qsi	Incoming solar irradiance
R	Rainfall
WQ_soil	Water Quality soil module
soil_WL/SWL	Soil water level elevation above the semipermeable layer
soil_moist	Soil moisture
Poro_soil	Soil porosity
AL	Above layer
BL	Below layer
GWRD	Groundwater level fluctuations, groundwater recharge and discharge

1082

1083

1084

1085 **Appendix C**

1086

1087 We show how we assess seasonal factors ( $f_{y,i}$ ) for different years in this study. Equation (4) can

1088 be written as:

1089

1090  $G_{y,i} = G \times f_{y,i}$  (C1)

1091

1092 For each year ( $y$ ),  $f_{y,i}$  for the first ( $f_{y,1}$ ) and second ( $f_{y,2}$ ) part of the sine function ( $G$ ), where

1093  $G \geq 0$  and  $G < 0$  respectively, were defined as:





1094

$$1095 \quad \begin{cases} \text{if } G \geq 0 [i = 1] \text{ then } f_{y,1} = x \\ \text{if } G < 0 [i = 2] \text{ then } f_{y,2} = y \end{cases} \quad (C-2)$$

1096

1097  $G$  is the sine function representing the annual fluctuations in soil water level. So, for  $n$  years

1098 there are  $n \times 2 f_{y,i}$  values. The default values for  $f_{y,i}$  are 1 and the default values can be changed

1099 for each year and for first and second parts in each year independently. Calculated  $G_{y,i}$  in each

1100 time step add or subtracted to or from the total soil moisture depend on the its sign. The values

1101 for the sine function parameters are in Fig. C1. The verified sine function time series along with

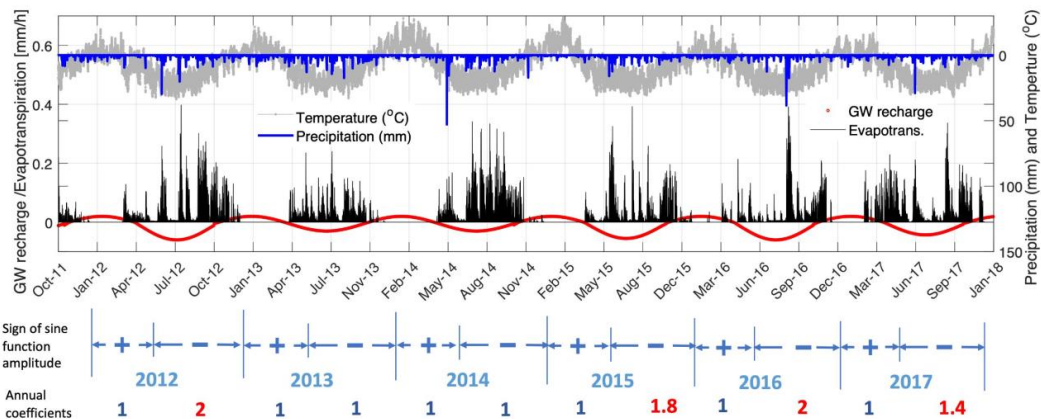
1102 time series of temperature, precipitation and calculated evapotranspiration are shown in Fig. C1.

1103 In this figure it is obvious that in years 2012 and 2015 to 2017 the warm season amplitudes are

1104 larger. The ET values are happen more in the warm seasons (growing seasons). Also it can be

1105 seen that the seasonal oscillation in sine function is very similar to the temperature general

1106 oscillations.



1107

1108 Figure C1 Time series of the adjustable sine function along with the time series of calculated evapotranspiration, temperature

1109 and precipitation during the study period from Oct 2011 to Sept 2018.